ORIGINAL ARTICLE

Ring-opening polymerization of cyclic esters by 3- and 4-pyridinyl Schiff base Zn(II) and Cu(II) paddlewheel complexes: kinetic, mechanistic and tacticity studies

Damilola C. Akintayo [a], **Wisdom A. Munzeiwa** [b], **Sreekantha B. Jonnalagadda** [a], **Bernard Omondi** [c],*

[a] School of Chemistry & Physics, University of KwaZulu-Natal, Westville Campus, Private Bag X54001, Durban 4000, South Africa
[b] Chemistry Department, Bindura University of Science Education, Private Bag 1020, Bindura, Zimbabwe
[c] School of Chemistry & Physics, University of KwaZulu-Natal, Pietermaritzburg Campus, Private Bag X01, Scottville 3209, South Africa

Abstract We have previously reported a series of highly active N,O-Amino-phenolate Mg(II) and Zn(II) Schiff base complexes for caprolactone and lactide polymerization (Munzeiwa, Nyamori, and Omondi, 2019). Herein we report carboxylate Zn(II) and Cu(II) pyridinyl Schiff base complexes and in particular, those whose ligands have substituents slightly situated away from the metal center. The complexes were fully characterized and for some fully by single-crystal X-ray diffraction studies. The ligands were confirmed to be monodentate and their complexes have the famous paddlewheel conformation. The carboxylate complexes were found to initiate the polymerization of ε-caprolactone and lactides in the presence or absence of alcohol, yielding low molecular weight polymers between 1.27 and 5.65 kg mol^{-1}, with broad $\tilde{a}$ between 1.7 and 2.0. The Zn(II) complexes were more reactive than their Cu(II) analogues. Activity of the complexes seems to have been influenced by the electronic properties of the substituents with the highest apparent rate constant, k_{app} of 0.4043 h^{-1}, being obtained for the complex of the ligand with an electron-withdrawing group (chloro). The complex was used to investigate activity and stereo-selectivity towards the ring-opening polymerization of L-lactide and rac-lactide. Tetrad analysis of the polylactides obtained

* Corresponding author.
  E-mail address: owaga@ukzn.ac.za (B. Omondi).
Peer review under responsibility of King Saud University.

ELSEVIER **Production and hosting by Elsevier**

from homonuclear ^{1}H and ^{13}C NMR afforded isotactic PLA with ∟-LA and heterotactic (Pr = 0.68) stereo-block PLA with *rac*-LA.

1. Introduction

Environmental pollution arising from non-biodegradable polymers obtained from petroleum sources has remained a global concern (Mittal, 2012), leading to the increased need to develop sustainable polymeric materials (Scott, 2002; Mecking, 2004). The current sustainable polymers are easy to synthesize by the ring-opening polymerization (ROP) of their monomers using metal complexes as initiators (Wu et al., 2006). Poly-lactide (PLA) and poly-caprolactone (PCL) are examples of the most prominently used alternatives and are biocompatible and biodegradable (Zhang, 2015). PLAs and PCLs have found usefulness in electronic devices (Jürgensen et al., 2016), packaging (Hong et al., 2016) and drug delivery (Nair and Laurencin, 2007; Middleton and Tipton, 2000).

Several metal catalyst such as zinc (Nuñez-Dallos et al., 2017; Walton et al., 2014; Roberts et al., 2012), aluminum (Kireenko et al., 2015; Sumrit et al., 2016; Liu and Ma, 2014; Zhang et al., 2016; Liu et al., 2001), copper (Ahn et al., 2017; Fortun et al., 2015; Li et al., 2013), calcium (Colwell et al., 2015; Chen et al., 2012; Range et al., 2008), bismuth(Bonné et al., 2017), lanthanides (Sheng et al., 2007; Liu et al., 2007; Rosal et al., 2011; Li et al., 2012; Nie et al., 2012) and magnesium (Devaine-Pressing et al. 2015; D'Auria et al. 2017; Balasanthiran et al. 2016) have been employed for the synthesis of polyesters with tin(II) octanoate being the preferred commercially available catalyst. Although octanoic acid is biodegradable, the oxidation of Sn(II) to Sn(IV) is of grave consequence to aquatic organisms and the environment (Tanzi et al. 1994), limiting its usage in medicine. Thus, benign metals like zinc and copper can be used as alternatives to toxic metal-based complexes because they are biocompatible and relatively cheap.

The chelating atoms and substituent groups in the ligand architecture have been reported to influence catalytic activity of the complexes formed significantly. Nitrogen donor ligands such as piperidine (Chen et al., 2015), pyrazole (Appavoo et al. 2014; Castro-Osma et al. 2013), formamidine (Munzeiwa et al., 2018; Munzeiwa et al., 2017; Akpan et al. 2016b, 2016a), pyridine(Zikode et al., 2016; Kireenko et al. 2015), ketiminate (Keram and Ma, 2017; Chen et al., 2015; Whitehorne and Schaper, 2013; El-Zoghbi et al., 2013), among others, have been employed for the stabilization of metal complexes used to initiate the ROP of cyclic esters. The ease in synthesis and their excellent coordination capability make nitrogen donor ligands an attractive catalytic frame for ROP studies. Carboxylate complexes of *N,N'*-diaryl formamidine ligands (Akpan et al. 2016a; Munzeiwa et al., 2017), and pyrazole (Appavoo et al. 2014; Sarma et al., 2009), have been reported to initiate the ROP of ε-CL and LA efficiently. They are known to deliver various coordination modes that determine the stability and reactivity of the complexes. The carboxylate ligands are an important class of organic compounds with

excellent biological properties (Sirajuddin et al. 2020). They are also known to enhance the catalytic activity of homoleptic metal complexes (Qi et al. 2015). In this report, we have explored the potential of pyridinyl Schiff base ligands to stabilize Zn(II) and Cu(II) acetate complexes, which provides the M—O bond required to initiate the polymerization of cyclic esters (Fliedel et al. 2015). The ligands were designed in a manner as to remove the immediate influence of the electronic groups on the metal center.

2. Experimental

2.1. Materials and reagents

Schlenk techniques were used for all manipulations using argon as the choice gas. All solvents, tetrahydrofuran (THF) 98%, dichloromethane (DCM) (99%) and hexane (98%) were obtained from Sigma-Aldrich, all dried from a sodium-benzophenone mixture. Metal salts [Cu(OAc)$_2$·2H$_2$O and Zn (OAc)$_2$·2H$_2$O], 3-pyridinecarboxaldehyde (98%), 4-pyridinecarboxaldehyde (98%), *p*-toluidine, 4-chloroaniline, 2,6-dimethylaniline (99%), 2,6-diisopropylaniline (97%), aniline (99%), ε-caprolactone (ε-CL) (97%), ∟-lactide (∟-LA) (98 %) and *rac*-lactide (*rac*-LA) (98%) were also obtained from Sigma-Aldrich and used without further purification.

2.2. Instrumentation

^{1}H- and ^{13}C NMR spectra were measured at room temperature using a Bruker 400 MHz spectrometer. ^{1}H- and ^{13}C NMR data were recorded in CDCl$_3$, with a residual internal solvent signal of CDCl$_3$ as 7.26 and 77.00 ppm, respectively. IR spectra were obtained on a PerkinElmer Universal ATR spectrum 100 FT-IR spectrometer. Mass spectra of the compounds were obtained from a Water synapt GR electrospray positive spectrometer. UV spectra were obtained using UV-3600 Shimadzu UV–VIS-NIR spectrophotometer.

2.3. Synthesis of the Schiff base ligands

Solvent-free grinding was employed for the synthesis of ligands **L1** - **L10** using the procedure described in literature (Njogu et al., 2017). Pyridinecarboxaldehyde (1 mmol, 0.107 g) mixed with *p*-toluidine (1 mmol, 0.107 g), 4-chloroaniline (1 mmol, 0.127 g), 2,6-dimethylaniline (1 mmol, 0.121 g), 2,6-diisopropylaniline (1 mmol, 0.177 g) and aniline (1 mmol, 0.093 g) were grinded with a mortar and pestle for 10 – 15 min. The products were dried in *vacuo* to completely remove the water. (E)-1-(pyridin-4-yl)-*N*-(p-tolyl)methanimine **L1**, (E)-N-(2,6-diisopropylphenyl)-1-(pyridin-4-yl)methanimine **L2**, (E)-N-(4-chlorophenyl)-1-(pyridin-4-yl)methanimine **L3**, (E)-N-(2,6-dimethylphenyl)-1-(pyridin-4-yl)methanimine **L4**, (E)-N-phenyl-1-(pyridin-4-yl)methanimine **L5**, (E)-1-(pyridin-3-y

l)-N-(p-tolyl)methanimine **L6**, (E)-N-(2,6-diisopropylphenyl)-1-(pyridin-3-yl)methanimine **L7**, (E)-N-(4-chlorophenyl)-1-(pyridin-3-yl)methanimine **L8**, (E)-N-(2,6-dimethylphenyl)-1-(pyridin-4-yl)methanimine **L9** and (E)-N-phenyl-1-(pyridin-4-yl)methanimine **L10** shown in Fig. 1 were obtained in excellent yield (97–98%).

2.4. Synthesis of metal complexes

The Schiff base metal complexes (**1** – **13**) were prepared in methanol solution at ambient temperature via the reaction between the metal(II) acetate and the respective Schiff base ligand synthesized using reported literature protocol (Sarma et al., 2009). Generally, the metal carboxylates were obtained by the gradual addition of either ethanolic (ca. 10 mL) Zn (II) acetate (1 mmol, 0.219 g) or Cu(II) acetate (1 mmol, 0.2 g) to a solution of ligands **1**–**10** (1 mmol) respectively in ethanol (ca. 10 mL) under constant stirring for 6 h. The resulting solids were filtered using a vacuum filter to obtain the crude product, which was recrystallized from dichloromethane (DCM).

2.4.1. [Zn(CH₃COO)₂(L1)]₂ (1)

2.4.1. [Zn(CH₃COO)₂(L1)]₂ (1)

Complex **1** was synthesized using [Zn(OAc)₂] (1 mmol) and **L1** (1 mmol) and isolated as a green solid. Yield: 83 %, M.Pt.: 175–176 °C. ^{1}H NMR (400 MHz, CDCl₃): δ ppm 2.07 (6H, s), 2.39 (3H, s), 7.22 (4H, q, J = 7.33 Hz), 7.90 (2H, d, J = 5.88 Hz), 8.51 (1H, s), 8.84 (2H, d, J = 5.75 Hz). ^{13}C NMR (400 MHz, CDCl₃): δ ppm 21.14, 22.76, 121.15, 123.16, 130.01, 137.88, 145.10, 147.71, 150.10, 155.31, 180.26. IR: υ (cm^{-1}) 3005 υ(C−H) str., 1626 υ(C=O) asym. str., 1422 υ(C=O) sym. str., 687 υ (M−O) str., 323 υ (M−N) str. MS (ESI-TOF) m/z: Calcd. for: [Zn(CH₃COO)₂(L1)]₂: 759.4420, found: [M$^+$ + 5H] 765.1444 (90 %) [M$^+$ − C₂H₃O₂] 701.0923 (100 %). Anal. Calcd. (%) for C₃₄H₃₈N₄O₉Zn₂: C, 52.53; H, 4.93; N, 7.21. Found: C, 52.70, H, 4.74, N, 7.36.

2.4.2. [Cu(CH₃COO)₂(L1)]₂ (2)

Complex **2** was synthesized using [Cu(OAc)₂] (1 mmol) and **L1** (1 mmol) and isolated as a green solid. Yield: 84 %, M.Pt.: 233–234 °C. IR: υ (cm^{-1}) 3004 υ(C−H) str., 1626 υ(C=O) asym. str., 1422 υ(C=O) sym. str., 823, 676 υ (M−O) str., 349 υ (M−N) str. MS (ESI-TOF) m/z: Calcd. for [Cu(CH₃COO)₂(L1)]₂: 755.7740, found: [M$^+$ + 3H] 758.2207 (2 %), [M$^+$ - C₄H₆O₄ + 2Na] 684.2031 (5 %). Anal. Calcd. (%)

for C₃₄H₃₆N₄O₈Cu₂: C, 54.03; H, 4.80; N, 7.41. Found: C, 54.24, H, 4.84, N, 7.44.

2.4.3. [Zn(CH₃COO)₂(L2)]₂ (3)

Complex **3** was synthesized using [Zn(OAc)₂] (1.00 mmol) and L2 (1.00 mmol) and isolated as a green solid. Yield: 74 %, M. Pt. 194–195 °C. ^{1}H NMR (400 MHz, CDCl₃): δ ppm 1.17 (12H, d, J = 6.85 Hz), 2.07 (6H, s), 2.87 (2H, m, J = 6.83 Hz), 7.17 (3H, q, J = 4.78 Hz), 7.92 (2H, d, J = 5.90 Hz), 8.24 (1H, s), 8.88 (2H, d, J = 5.67 Hz). ^{13}C NMR (400 MHz, CDCl₃): δ ppm 22.81, 23.40, 28.06, 122.99, 123.21, 125.08, 137.01, 148.11, 150.30, 159.38, 180.45. IR: υ (cm^{-1}) 2969 υ(C−H) str., 1626 υ(C=O) asym. str., 1421 υ (C=O) sym. str., 760, 676 υ (M−O) str., 366 υ (M−N) str. MS (ESI-TOF) m/z: Calcd. for [Zn(CH₃COO)₂(L2)]₂: 899.7120, found: [M$^+$ - C₄H₆O₄] 797.2065 (45 %), [Zn(L2) C₂H₃O₂] 658.0739 (27 %), 595.2869 [Zn(L₂)] 595.2869 (100 %). Anal. Calcd. (%) for C₄₄H₅₈N₄O₉Zn₂: C, 57.59; H, 6.37; N, 6.11. Found: C, 57.65, H, 6.31, N, 5.91.

2.4.4. [Cu(CH₃COO)₂(L2)]₂ (4)

Complex **4** was synthesized using [Cu(OAc)₂] (1.00 mmol) and L2 (1.00 mmol) and isolated as a green solid. Yield: 78 %, M. Pt. 230–231 °C. IR: υ (cm^{-1}) 2959 υ(C−H) str., 1626 υ(C=O) asym. str., 1422 υ(C=O) sym. str., 756, 676 υ (M−O) str., 360 υ (M−N) str. MS (ESI-TOF) m/z: Calcd. for [Cu(CH₃COO)₂(L2)]₂: 896.0440, found: [M$^+$] 894.9740 (2 %), [M − C₄H₆O₄] 793.0817 (5 %), [Cu(L2)₂] 595.2856(100 %). Anal. Calcd. (%) for C₄₄H₅₆N₄O₈Cu₂: C, 58.98; H, 6.30; N, 6.25. Found: C, 58.76, H, 6.24, N, 6.29.

2.4.5. [Zn(CH₃COO)₂(L3)]₂ (5)

Complex **5** was synthesized using [Zn(OAc)₂] (1.00 mmol) and L3 (1.00 mmol) and isolated as a yellow solid. Yield: 92 %, M. Pt. 193–194 °C. ^{1}H NMR (400 MHz, CDCl₃): δ ppm 2.05 (6H, s), 7.22 (2H, d, J = 8.59 Hz), 7.40 (2H, d, J = 8.58 Hz), 7.89 (2H, d, J = 4.93 Hz), 8.48 (1H, s), 8.84 (2H, d, J = 5.35 Hz). ^{13}C NMR (400 MHz, CDCl₃): δ ppm 22.87, 116.36, 122.39, 122.87, 128.23, 129.07, 129.51, 133.10, 143.83, 148.96, 150.38, 151.23, 157.31, 180.49, 191.26. IR: υ (cm^{-1}) 3071 υ(C−H) str., 1608 υ(C=O) asym. str., 1422 υ(C=O) sym. str., 714 υ (M−O) str., 373 υ (M−N) str. MS (ESI-TOF) m/z: Calcd. for [Zn(CH₃COO)₂(L3)]₂: 800.2720, found: [M$^+$ + K] 840.8028 (2 %), [Zn(L3)C₂H₃O₂] 542.9744 (100 %). Anal. Calcd. (%) for C₃₂H₃₂N₄O₉Cl₂Zn₂: C, 46.97; H, 3.94; N, 6.85. Found: C, 46.84, H, 3.69, N, 6.65.

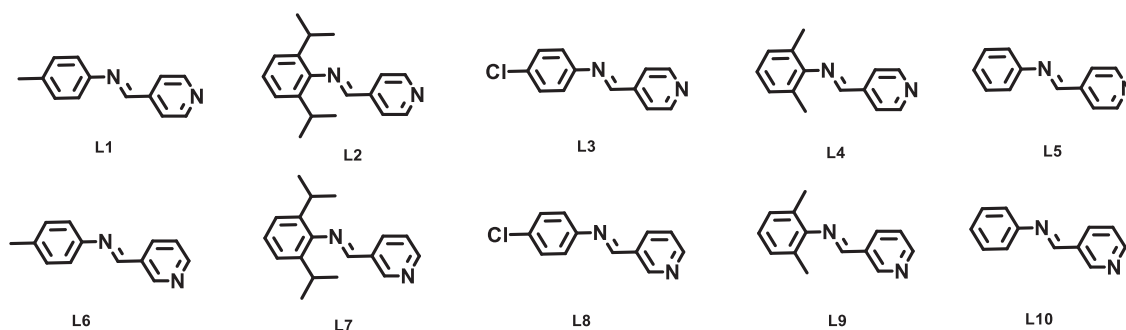**Fig. 1** Schiff base ligands **L1** – **L10** used in this study.

2.4.6. [Cu(CH₃COO)₂(L3)]₂ (6)

Complex **6** was synthesized using [Cu(OAc)₂] (1.00 mmol) and L3 (1.00 mmol) and isolated as a green solid. Yield: 94 %, M. Pt. 229–230 °C. IR: υ (cm^{-1}) 3059 υ(C─H) str., 1602 υ(C═O) asym. str., 1421 υ(C═O) sym. str., 700 υ (M─O) str., 358 υ (M─N) str. MS (ESI-TOF) m/z: Calcd. for [Cu(CH₃COO)₂(L3)]₂: 796.6040, found: [M$^+$] 796.7462 (2 %), [Cu(L3)C₂H₃O₂] 341.0558 (100 %). Anal. Calcd. (%) for C₃₂H₃₀N₄O₈Cl₂Cu₂: C, 48.25; H, 3.80; N, 7.03. Found: C, 48.31, H, 3.81, N, 7.03.

2.4.7. [Cu(CH₃COO)₂(L4)]₂ (7)

Complex **7** was synthesized using [Cu(OAc)₂] (1.00 mmol) and L4 (2.00 mmol) and isolated as a green solid. Yield: 75 %, M. Pt. 242–243 °C. IR: υ (cm^{-1}) 2992 υ(C─H) str., 1614 υ(C═O) asym. str., 1422 υ(C═O) sym. str., 756, 678 υ (M─O) str., 349 υ (M─N) str. MS (ESI-TOF) m/z: Calcd. for [Cu(CH₃COO)₂(L4)]₂: 783.8280, found: [Cu₂(L4)(C₄H₆O₄)] 454.6789 (4 %), [Cu(L4)C₂H₃O₂] 327.0410 (90 %). Anal. Calcd. (%) for C₃₆H₄₀N₄O₈Cu₂: C, 55.16; H, 5.14; N, 7.15. Found: C, 54.89, H, 5.14, N 7.24.

2.4.8. [Cu(CH₃COO)₂(L5)]₂ (8)

Complex **8** was synthesized using [Cu(OAc)₂] (1.00 mmol) and L5 (2.00 mmol) and isolated as a green solid. Yield: 75 %, M. Pt. 229–230 °C. IR: υ (cm^{-1}) 3071 υ(C─H) str., 1614 υ(C═O) asym. str., 1422 υ(C═O) sym. str., 676 υ (M─O) str., 360 υ (M─N) str. MS (ESI-TOF) m/z: Calcd. for [Cu(CH₃COO)₂(L5)]₂: 727.7200, found: [Cu(L5)(C₂H₃O₂)₃] 4,409,498 (7 %), [Cu(L5)C₄H₆O₄ + Na] 386.0522 (5 %), [Cu(L5)C₂H₃O₂ + Na] 327.0405 (94 %). Anal. Calcd. (%) for C₃₂H₃₂N₄O₈Cu₂: C, 52.82; H, 4.43; N, 7.70% Found: C, 52.96, H, 4.58, N, 7.65.

2.4.9. [Cu(CH₃COO)₂(L6)]₂ (9)

Complex **9** was synthesized using [Cu(OAc)₂] (1.00 mmol) and L6 (2.00 mmol) and isolated as a green solid. Yield: 79 %, M. Pt. 207–208 °C. IR: υ (cm^{-1}) 3004 υ(C─H) str., 1614 υ(C═O) asym. str., 1422 υ(C═O) sym. str., 756, 676 υ (M─O) str., 349 υ (M─N) str. MS (ESI-TOF) m/z: Calcd. for [Cu(CH₃COO)₂(L6)]₂: 755.7740, found: [M$^+$] 756.8930 (3 %), [Cu(L6)₂] 448.9847 (15 %), [Cu(L6)C₂H₃O₂ + Na] 341.0566 (45 %). Anal. Calcd. (%) for C₃₄H₃₆N₄O₈Cu₂: C, 54.03; H, 4,80; N, 7.41. Found: C, 53.81, H, 4.83, N, 7.51.

2.4.10. [Cu(CH₃COO)₂(L7)]₂ (10)

Complex **10** was synthesized using [Cu(OAc)₂] (1.00 mmol) and L7 (2.00 mmol) and isolated as a green solid. Yield: 88 %, M.Pt. 219–220 °C. IR: υ (cm^{-1}) 2969 υ (C─H) str., 1626 υ(C═O) asym. str., 1422 υ(C═O) sym. str., 756, 676 υ (M─O) str., 349 υ (M─N) str. MS (ESI-TOF) m/z: Calcd. for [Cu(CH₃COO)₂(L7)]₂: 896.0440, found: [M$^+$] 894.9740 (2 %), [M – C₄H₆O₄] 793.0817 (5 %), [Cu(L7)₂] 595.2856 (100 %). Anal. Calcd. (%) for C₄₄H₅₆N₄O₈Cu₂: C, 58.98; H, 6.30; N, 6.25. Found: C, 58.87, H, 6.28, N 6.26.

2.4.11. [Cu(CH₃COO)₂(L8)]₂ (11)

Complex **11** was synthesized using [Cu(OAc)₂] (1.00 mmol) and L8 (2.00 mmol) and isolated as a green solid. Yield: 83 %, M.Pt. 227–228 °C. IR: υ (cm^{-1}) 3060 υ (C─H) str., 1602 υ(C═O) asym. str., 1422 υ(C═O) sym. str., 699 υ (M─O) str., 360 υ (M─N) str. MS (ESI-TOF) m/z: Calcd. for [Cu(CH₃COO)₂(L8)]₂: 796.6040, found: [M$^+$] 796.1827 (2 %), [M$^+$ - C₄H₆O₄Cu] 610.1814 (10 %), [Cu(L8)C₂H₃O₂] 341.0245 (90 %). Anal. Calcd. (%) for C₃₂H₃₀N₄O₈Cl₂Cu₂: C, 48.25; H, 3.80; N, 7.03. Found: C, 48.15, H, 3.72, N, 7.12.

2.4.12. [Cu(CH₃COO)₂(L9)]₂ (12)

Complex **12** was synthesized using [Cu(OAc)₂] (1.00 mmol) and L9 (2.00 mmol) and isolated as a green solid. Yield: 81 %, M.Pt. 220–221 °C. IR: υ (cm^{-1}) 2947 υ(C─H) str., 1614 υ(C═O) asym. str., 1422 υ(C═O) sym. str., 687 υ (M─O) str., 349 υ (M─N) str. MS (ESI-TOF) m/z: Calcd. for [Cu(CH₃COO)₂(L9)]₂: 783.8280, found: [M$^+$] 779.1495 (5 %), [M$^+$ - C₄H₆O₄Cu] 610.1840 (25 %). Anal. Calcd. (%) for C₃₆H₄₀N₄O₈Cu₂: C, 55.16; H, 5.14; N, 7.15. Found: C, 55.29, H, 5.23, N, 7.11.

2.4.13. [Cu(CH₃COO)₂(L10)]₂ (13)

Complex **13** was synthesized using [Cu(OAc)₂] (1.00 mmol) and L10 (2.00 mmol) and isolated as a green solid. Yield: 85 %, M.Pt. 209–210 °C. IR: υ (cm^{-1}) 3026 υ(C─H) str., 1614 υ(C═O) asym. str., 1421 υ(C═O) sym. str., 687 υ (M─O) str., 349 υ (M─N) str. MS (ESI-TOF) m/z: Calcd. for [Cu(CH₃COO)₂(L10)]₂: 727.7200, found: [(M$^+$ - C₄H₆O₄) + Na] 684.2028 (10 %), [Cu₂(L10)₂C₄H₆O₄] 610.1846 (35 %). Anal. Calcd. (%) for C₃₂H₃₂N₄O₈Cu₂: C, 52.82; H, 4.43; N, 7.70. Found: C, 52.67, H, 4.36, N, 7.56.

2.5. General procedure for ring-opening polymerization of ε-caprolactone (ε-CL) and lactide (LA)

All polymerization reactions were carried out using Schlenk techniques with argon as the gas. The required amount of the respective complex was added into a Schlenk tube containing the monomer ε-CL (1.14 g, 0.01 mol) and LA (1.44 g, 0.01 mol) in bulk and also in toluene (5 mL) immersed in a pre-heated oil bath at 110 °C to initiate the polymerization reaction. Samples were withdrawn at regular intervals using a syringe, and quenched quickly by dissolving in cooled CDCl₃ in an NMR tube for kinetic experiments. The conversion of polymerization was determined by ¹H NMR spectroscopy and was evaluated using Eqs. (1) and (2). For ε-CL, signal intensities at 4.0 ppm ($I_{4.0}$) for OCH₂ protons of PCL and signal intensities at 4.2 ppm ($I_{4.2}$) for ε-CL monomer using Eq. (1).

$$\frac{[Polymer]_t}{[Monomer]_o} \times 100 = \frac{I_{4.0}}{(I_{4.0} + I_{4.2})} \times 100 \tag{1}$$

For PLA, the integration values of the methine proton of the LA monomer and that of the PLA polymer were obtained using Eq. (2).

$$\frac{[Polymer]_t}{[Monomer]_o} \times 100 = \frac{I_{CHpolymer}}{(I_{CHmonomer} + I_{CHpolymer})} \times 100 \tag{2}$$

The peak areas of the polymer and monomer were used to deduce the conversion. The observed rate constants were extracted from the slope of the line of best fit from the plot of $\ln([M]_o/[M]_t)$ vs t.

2.6. Polymer characterization by size exclusion chromatography (SEC)

Molecular weights and polydispersity indexes ($Đ$) were determined by size exclusion chromatography (SEC) at the central analytical facilities, Stellenbosch University, South Africa. The samples were dissolved in tetrahydrofuran (THF) stabilized with butylated hydroxytoluene (BHT), giving a sample with a concentration of 2 mg ml^{-1}. Sample solutions were filtered via a syringe through 0.45 mm nylon filters before being subjected to analysis. The SEC instrument consists of a Waters 1515 isocratic HPLC pump, a Waters 717plus auto-sampler, a Waters 600E Paper system controller (run by Breeze Version 3.30 SPA) and a Waters in-line Degasser AF. A Waters 2414 differential refractometer was used at 30 °C in series along with a Waters 2487 dual wavelength absorbance UV/Vis detector operating at variable wavelengths·THF (HPLC grade stabilized with 0.125 % BHT) was used as the eluent at flow rates of 1 mL min^{-1}. The column oven was kept at 30 °C and the injection volume was 100 mL. Two PLgel (Polymer Laboratories) 5 mm Mixed-C (300 × 7.5 mm) columns and a pre-column (PLgel 5 mm Guard, 50 × 7.5 mm) were used. Calibration was done using narrow polystyrene standards ranging from 580 to 2 × 10^6 g mol^{-1}. All molecular weights were reported as polystyrene equivalents.

2.7. Molecular structure determination by single-crystal X-ray analysis

Crystal evaluation and data collection were done on a Bruker Smart APEXII diffractometer with Mo Kα radiation (I = 0. 71073 Å) fitted with an Oxford Cryostream low-temperature apparatus operating at 100 K for **7, 9, 10 and 11**. Reflections were collected at different starting angles and the *APEX*II program suite was used to index the reflections (Bruker, 2009a). Data reduction was performed using the *SAINT* (Bruker, 2009c) software, and the scaling and absorption corrections were applied using the *SADABS* (Bruker, 2009b) multi-scan technique. The structures were solved by the direct method using the *SHELXS* program and refined using the *SHELXL* program (Sheldrick, 2008). Graphics of the crystal structures were drawn using OLEX2 software (Dolomanov et al. 2009). Non-hydrogen atoms were first refined isotropically and then by anisotropic refinement with the full-matrix least squares method based on F^2 using *SHELXL* (Sheldrick, 2008). The crystallographic data and structure refinement parameters for complexes **7, 9, 10** and **11** are given in Table 1.

3. Results and discussion

3.1. Synthesis and spectroscopic studies of Schiff base ligands

The Schiff base ligands used in this work were prepared via mechanochemical procedure in which the aldehydes along with substituted aniline were ground for ten minutes using a mortar and pestle to obtain **L1 - L10** in good yields of 97 – 99 % (Scheme 1). The condensation reaction was followed using thin layer chromatography (TLC) and Fourier Transform Infrared (FT-IR) spectroscopy until the N—H and C═O bands from the reactants disappeared, confirming the completion of the

reaction. The crude product was dried in vacuo and further characterized by FT-IR spectroscopy which gave spectra with characteristic imine (C═N) bands around 1620–1640 cm^{-1}. The ^{1}H and ^{13}C NMR analyses of the Schiff base ligands revealed a singlet peak at about 8.20–8.44 ppm and 156 ppm, respectively, which corresponds to the formation of the imine bond (HC═N) commonly reported in the literature for Schiff bases (Dong et al. 2016; Munzeiwa et al., 2019; Köppl and Alt, 2000). The ^{1}H and ^{13}C NMR spectra of **L1- L10** are available in the supplementary information (Figs. S1 - S20).

3.2. Synthesis and spectroscopic studies of Zn(II) and Cu(II) carboxylates

Zn(II) and Cu(II) acetate (1:1) were added to methanolic solutions of the Schiff base ligands and stirred at room temperature for 6 h to produce the metal carboxylate complexes in good yields between 75 and 94% (Scheme 2). The characterization of the carboxylate complexes by IR, mass spectroscopy, and elemental analysis points to a dinuclear carboxylate system [MLn(CH$_3$COO)$_2$]$_2$. The Zn(II) complexes were further characterized with ^{1}H- and ^{13}C NMR (Figs. S21 - S26).

The ESI-MS spectra of complexes **1 – 13** gave molecular and fragment ions peaks confirming a metal to ligand to acetate ratio of M$_2$L$_2$Ac$_2$. For instance Zn(II) complex **1** revealed m/z peaks at 765.14, 701.09 and 515.09 which corresponds to (M$^+$ + 5H), [M$^+$ – C$_2$H$_3$O$_2$] and Zn(L1)(C$_2$H$_3$O$_2$) ions, respectively. The base peak observed at 701.09 matched the [M$^+$ – C$_2$H$_3$O$_2$] fragment (Fig. S37). Similarly, Cu(II) complex **10** revealed m/z peaks at 894.9 and 793.1 corresponding to the molecular ion (M$^+$) and the [M$^+$ – C$_4$H$_6$O$_4$] ion, respectively. The base peak observed at 595.5 matched the Cu(L7)$_2$ fragment which suggests the formation of the stable mononuclear species in dichloromethane solution (Fig. S38).

Analysis of the metal carboxylates by FTIR spectroscopy revealed bands between 323 and 373 cm^{-1} corresponding to the M—N$_{py}$ stretching frequency and between 676 and 714 cm^{-1} corresponding to M—O stretching frequencies. This is an indication of the coordination of the metal center to the pyridinyl N atom and the acetate O atom. The syn-syn bidentate bands of the coordinated carboxylate were observed between 1421 and 1422 cm^{-1} and between 1602 and 1626 cm^{-1}, respectively, in all the complexes, which resulted in a $\Delta\upsilon$ that lie in the range $180 \geq \Delta\upsilon \leq 205$ similar to reported paddle wheel geometry (Akpan et al. 2016b; Zhu et al. 2010; Selvakumar et al., 2008; Vagin et al., 2007).

Absorption spectra of **1, 3** and **5** in chloroform (Fig. 2a) and **2, 4, 6–13** in dichloromethane (Fig. 2b) were analyzed in the 200–450 nm wavelength range. Bands observed between 230 and 243 nm and 264 and 265 nm were assigned to π-π* transition and those in the range 322 to 336 nm assigned to n-π* as summarized in Table S1. The absorption spectra of the Zn(II) and Cu(II) complexes were found to be influenced by the nature and position of the ligand substituents. For example, three λ$_{max}$ values were generally observed with the complexes whose ligand contained both electron-donating (**1, 2** and **8**) and electron-withdrawing substituents (**5** and **6**) at the para position whereas two λ$_{max}$ values were obtained for ortho substituted and unsubstituted systems. The n-π* transition of the ortho substituted complexes (**3, 7, 10,** and **12**)

**Table 1**   Crystal data and structure refinement parameters for Complexes 7, 9, 10 and 11.

Complex	7	9	10	11
Empirical formula	$C_{36}H_{40}Cu_2N_4O_8$	$C_{34}H_{36}Cu_2N_4O_8$	$C_{44}H_{56}Cu_2N_4O_8$	$C_{30}H_{40}Cu_2Cl_2N_4O_8$
Formula weight	949.62	755.75	896.05	796.61
Temperature (K)	100	100	100.01	150.01
Wavelength (Å)	0.71073	0.71073	0.71073	0.71073
Crystal system	Monoclinic	Monoclinic	Monoclinic	Monoclinic
Space group	$P2_1/n$	$P2_1/n$	$P2_1/c$	$P2_1/n$
a/Å	7.472(4)	8.1473(6)	11.1007(2)	8.1456(3)
b/Å	12.097(10)	22.5828(16)	20.4534(3)	22.6010(7)
c/Å	23.845(18)	9.7106(7)	9.8008(2)	9.7027(3)
α, β, γ/°	90, 94.822(13), 90	90, 105.399(2), 90	90, 101.247(10), 90	90, 105.571(10), 90
V/Å^3	2148(3)	1722.5(2)	2182.51(7)	1720.70(10)
Z	4	2	2	2
ρ (calc.21) g/cm^3	1.469	1.457	1.3634	1.5374
μ /mm^{-1}	1.292	1.29	1.03	1.446
$F(000)$	972	780	941.7	814.3
Crystal size/mm^3	0.37 × 0.34 × 0.21	0.29 × 0.13 × 0.08	0.31 × 0.23 × 0.11	0.33 × 0.25 × 0.16
θ range for data collection/°	3.428 to 56.95	3.608 to 52.998	3.74 to 56.78	4.72 to 54.48
Index ranges	$-9 \le h \le 9$, $-16 \le k \le 16$, $-31 \le l \le 31$	$-10 \le h \le 9$, $-25 \le k \le 28$, $-12 \le l \le 10$	$-14 \le h \le 14$, $-22 \le k \le 27$, $-13 \le l \le 10$	$-10 \le h \le 10$, $-29 \le k \le 28$, $-12 \le l \le 12$
Reflections collected	30,277	9840	31,938	24,113
Independent reflections	5279 [R_{int} = 0.0440]	3410 [R_{int} = 0.0255]	5471 [R_{int} = 0.0213]	3844 [R_{int} = 0.0254]
Data / restraints / parameters	5279/0/230	3410/0/220	5471/0/268	3844/0/229
Goodness-of-fit on F2	1.224	1.029	1.033	0.964
R indices [I > 2sigma(I)] R_1, wR_2	0.0844, 0.1995	0.0303, 0.0730	0.0262, 0.0664	0.0254, 0.1049
R indices (all data) R_1, wR_2	0.0958, 0.2057	0.0427, 0.0782	0.0324, 0.0697	0.0288, 0.1105
Largest diff. peak/hole / e Å^{-3}	1.51/-1.36	0.38/-0.31	0.45/-0.36	0.38/-0.41
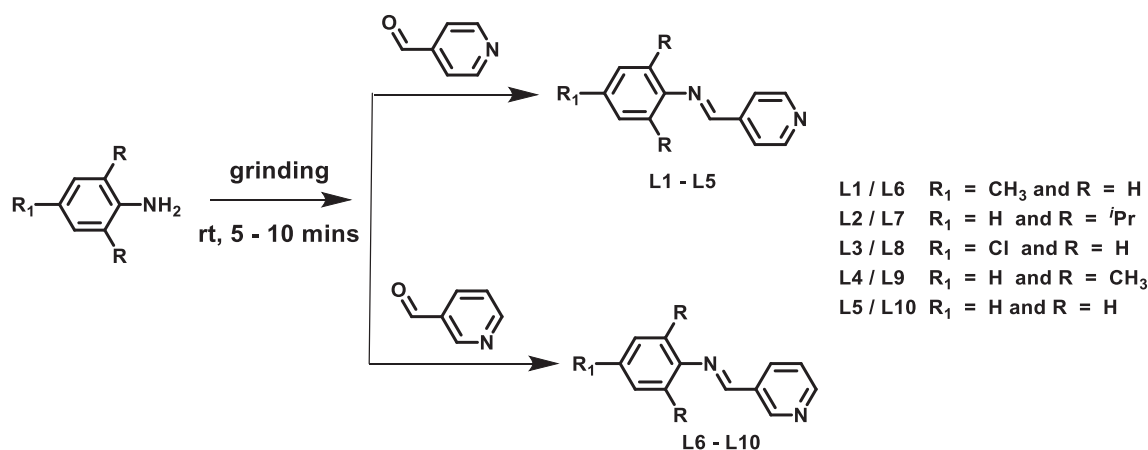
Scheme 1   Synthetic route for the preparation of Schiff base ligands L1 – L10.

experienced a hypochromic shift whereas the *para* substituted complexes (**1**, **5**, **6**, and **11**) experienced a hyperchromic shift.

The ^{1}H NMR analysis of the Zn(II) complexes displayed a characteristic singlet peak between 8.24 and 8.51 ppm corresponding to the imine proton (HC=N) of the Schiff base ligands. Additionally, the unique singlet peak observed around 2.07 ppm was assigned to the methyl proton of the bridging acetate, which confirmed the formation of the carboxylate complexes (Akpan et al. 2016b). The aromatic protons of the pyridinyl moiety shifted downfield upon coordination to the Zn(II) metal *via* the nitrogen atom in the pyridinyl pendant (Table S2). For instance, the ^{1}H NMR spectrum of complex

1 (Fig. S21) having a methyl substituent on the *para* position experienced the most significant shift (Table S2, entry 1) while complex **5** having a chloro substituent experienced the least shift (Table S2, entry 3). Similarly, ^{13}C NMR spectrum of complex **1** (Fig. S24) contained an additional carbon peak of the methyl of acetate observed at 22.76 ppm and the carbonyl peak at 180.26 ppm which established the formation of the complex with similar trends observed for all zinc complexes. The spectroscopic data obtained for the Zn(II) carboxylate complexes are consistent with results reported for similar carboxylate complexes (Akpan et al. 2016; Kumar et al., 2010). From the spectroscopic analysis, it is quite clear that all
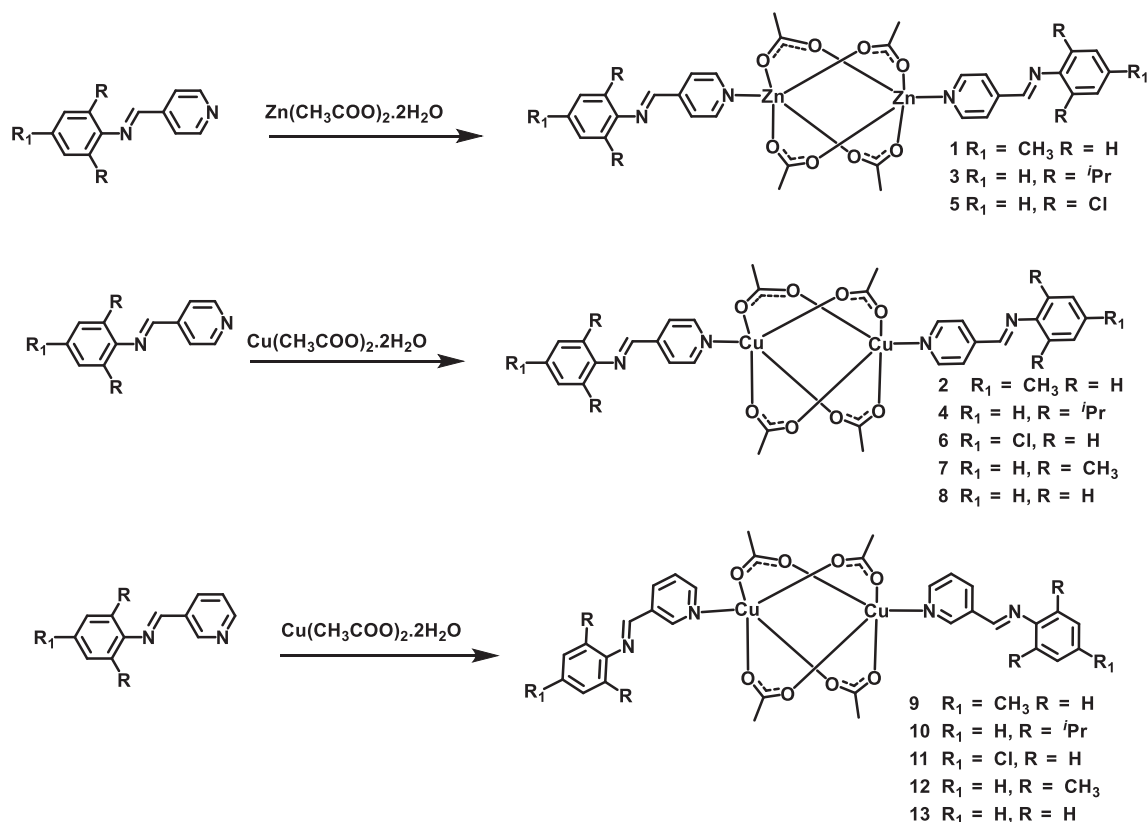
**Scheme 2** Synthesis of Zn(II) and Cu(II) pyridinyl complexes 1–13.
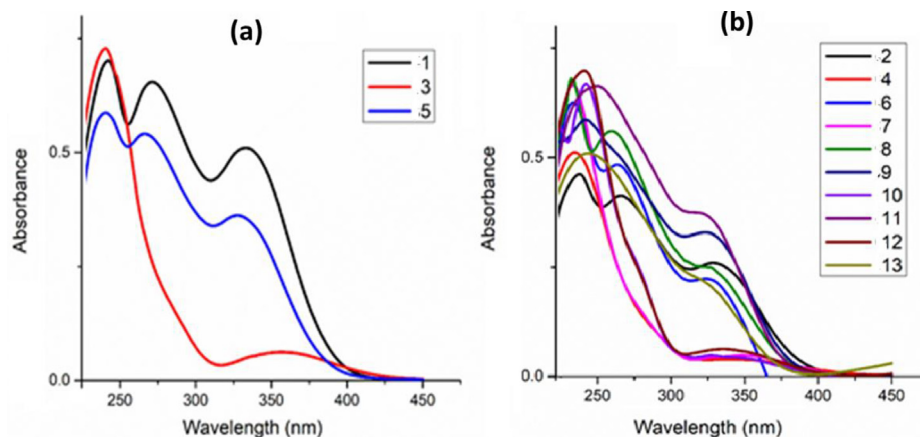
Fig. 2 Electronic absorption spectra of (a) complexes **1**, **3** and **5** in chloroform (b) complexes **2**, **4**, **6** – **13** in DCM.

complexes coordinated *via* the pyridinyl *N* atom, leaving the imine *N* atom uncoordinated as we intended (Adeleke et al., 2020).

3.3. Molecular structure of 7, 9, 10 and 11

The crystals of complexes **7, 9, 10 and 11** were all acquired by vapor diffusion of hexane into complex dichloromethane solutions. Their molecular structures obtained by single-crystal X-ray diffraction studies and are displayed in Fig. 3a - d with selected bond distances and angles summarized in Table 2. All complexes are neutral, and paddlewheel in the solid-state,

and each has only half a molecule in their asymmetric units. The other half in each case is generated through a center of inversion situated at the center of a Cu(II)--- Cu(II) supported interaction located at (ø ø ø), (0 1 0), (ø 1 0) and (0 ø ø) for complexes **7, 9, 10** and **11**, respectively. These cuprophilic Cu (II)-----Cu(II) interactions have distances equal to 2.6141(1) Å, 2.6280(3) Å, 2.6252(2) Å and 2.6270(3) Å which aligns with similar paddle wheel conformations in literature (Munzeiwa et al., 2018; Mosae Selvakumar et al. 2013; Attandoh et al., 2014). In all five complexes the carboxylate anions bridge the two Cu(II) centers in a bidentate bridging mode. The ligand coordinates to the Cu(II) center through the pyridinyl N atom,
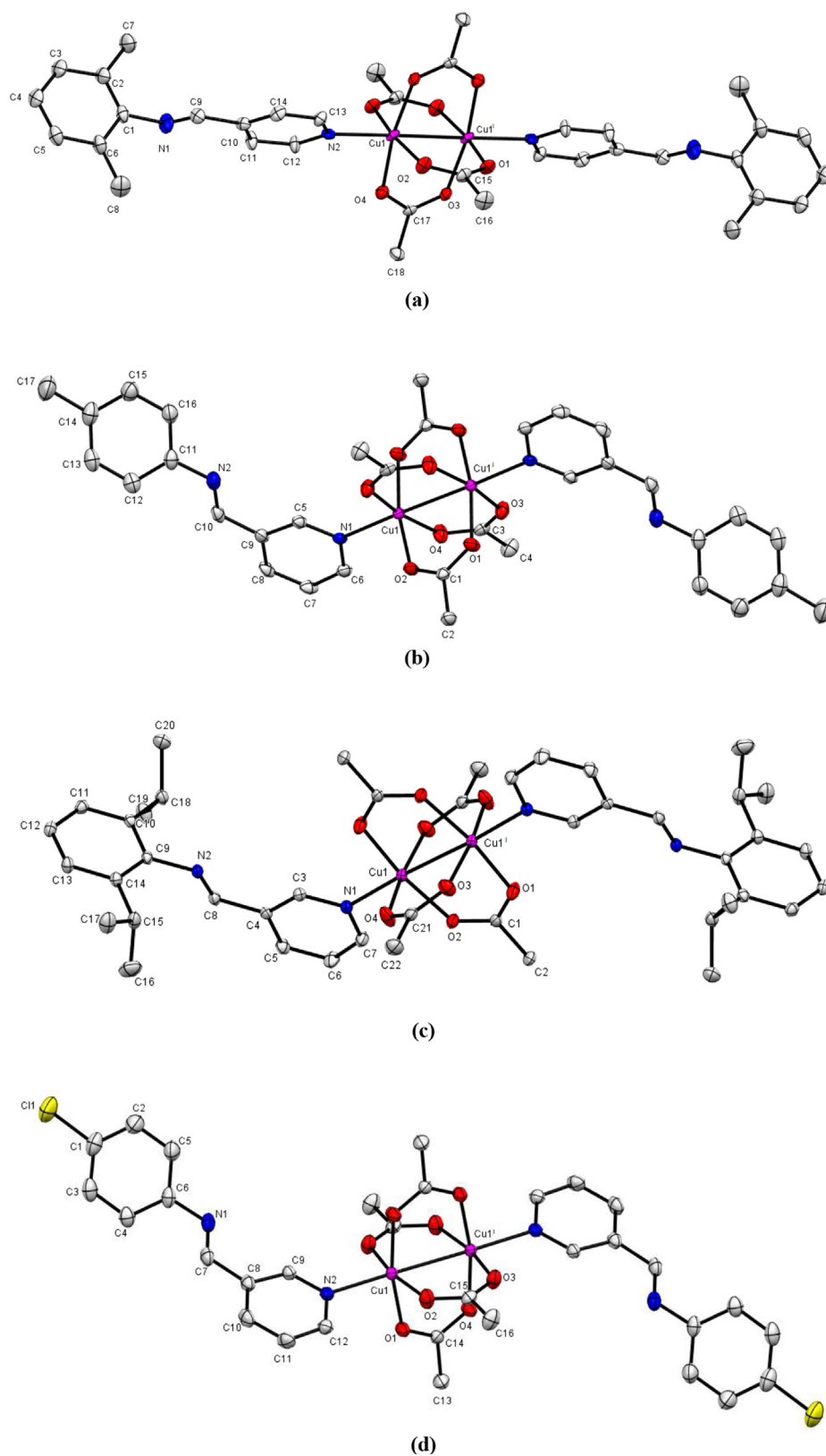
Fig. 3 Molecular structure of complexes (a) **7** and (b) **9**, (c) **10** and (d) **11** with thermal ellipsoids drawn at 50% probability level. Hydrogen atoms are omitted for clarity.

with Cu—N distances of 2.170(5), 2.1738(18), 2.2104(12) and 2.1774(13), for **7, 9, 10** and **11**, respectively. In doing so, the geometry around the Cu(II) centers is distorted octahedron in which four O atoms occupy the base of the equatorial posi-

Table 2 Selected bond lengths and bond angles for complexes **7**, **9**, **10** and **11**.

	7	9	10	11
Bond length [Å]				
Cu—O	1.962(4)	1.963(2)	1.962(1)	1.9678(12)
	1.976(4)	1.973(2)	1.970(1)	1.9729(12)
Cu—N$_{py}$	2.170(5)	2.174(2)	2.210(1)	2.1774(13)
Angles [°]				
O—Cu—O	89.2(2)	88.41(6)	88.29(5)	88.29(5)
	89.9(2)	90.74(6)	90.90(5)	90.58(6)
O—Cu—N$_{py}$	92.7(2)	94.82(7)	93.89(4)	95.02(5)
	98.3(2)	96.59(6)	97.55(5)	96.41(5)
Cu—Cu	2.6141(1)	2.6280(3)	2.6252(2)	2.6270(3)

Symmetry operators: i = −x, 1−y, 1−z for **7**, −x, 2−y, −z for **9**, 1−x, 2−y, −z for **10** and −2−x, 1−y, 1−z −x, for **11**.

tions while the pyridinyl N atom occupies the apex of the pyramid. The O—Cu—O bond angles are near orthogonal and so are the N—Cu—O bond angles.

Complexes **9** and **11** are isostructural considering the similarity in the unit-cell parameters even though the unit-cell volume of **9** is slightly higher than that of **11** (Table 1). A quantitative isostructural analysis was obtained using *Mercury* (CSD version 5.41) which gave a root mean square deviation of 0.0347 Å from an overlay of the two structures (Fig. S27). Further to this, the molecular packing of complexes **9** and **11** (Figs. S28 and S29) as viewed along the crystallographic a-axis also show a level of similarity.

4. Ring-opening polymerization of ε-CL and LAs

The catalytic activity of complexes **1 – 13** was studied for ε-CL and LAs polymerization in bulk and in toluene. (Table 3). The reactions were done at 110 °C using a [monomer]/[catalyst] ratio of 200:1. ^{1}H NMR analysis of the samples drawn from the reaction mixture gave conversions of 92 – 99 % between 12 and 120 h. Generally, Zn(II) complexes were more active than their Cu(II) analogue (Table 3, entries 2, 4 and 6) due to the polarity of the M—O bond (Akpan et al. 2016b) The low activity and slow initiation efficiency as evidenced by longer induction periods of Cu(II) analogues can be alluded to the structural paddle-wheel conformation which is normally stable. Although, the same structure is also observed with the Zn(II) complexes, but it appears that the Zn—O bonds is labile coupled with the greater nucleophilicity of Zn(II) in contrast to Cu(II). The slow onset of polymerization in paddlewheel structures can also be as a result of pro-catalyst rearranging to generate active species (Munzeiwa et al., 2018). In such an instance, we presume the catalyst are functioning as both initiators and catalysts, hence terms interchangeably used *vide infra*).

4.1. Kinetics of ROP reactions of ε-CL and LAs

A common observation reported for paddlewheel carboxylates is the slow onset of their polymerization in bulk at elevated temperature (Attandoh et al., 2014; Akpan et al. 2016b; Munzeiwa et al., 2018). This is because of the conformation changes experienced by the catalyst in the formation of the

Table 3 Summary of polymerization data of ε –CL and LAs for complexes **1 – 13**.[a]

Entry	Complex	[M]$_0$:[I]$_0$	Time (h)	[b]Conv (%)	[c]M$_{n(calc)}$ (kg mol^{-1})	[d]M$_{n(NMR)}$ (kg mol^{-1})	k_{app} (h^{-1})
1	**1**	200:1	45	99	22.6	4.86	0.1006
2	**2**	200:1	60	98	22.3	2.75	0.0953
3	**3**	200:1	14	98	22.6	5.65	0.3001
4	**4**	200:1	96	97	22.3	3.01	0.0707
5	**5**	200:1	12	99	22.6	5.08	0.4043
6	**6**	200:1	120	92	22.1	2.22	0.0328
7	**7**	200:1	55	99	22.3	3.20	0.1147
8	**8**	200:1	90	99	22.6	3.84	0.0597
9	**9**	200:1	60	99	22.1	2.08	0.0931
10	**10**	200:1	70	98	22.3	3.16	0.0612
11	**11**	200:1	120	97	22.1	2.36	0.0423
12	**12**	200:1	90	98	22.3	2.84	0.0751
13	**13**	200:1	60	98	22.6	4.46	0.0696
14	[e]**5**	200:1	20	95	27.5	1.27	0.1518
15	[f]**5**	200:1	20	97	28.1	3.35	0.2513

[a]Polymerization conditions: 110 °C, Bulk, One equivalent of the catalyst equal to [M(OAc)$_2$(L)]$_2$, [b,d] Determined from NMR, [c] M$_n$ calculated from the M$_{wt}$ of monomer × [M]$_0$:[I]$_0$ × Conv., [e] $_L$-LA and [f] *rac*-LA in toluene.

transition state (Motreff et al. 2012). Kinetic studies of samples withdrawn at regular intervals are usually conducted to gain insight into the polymerization mechanism and reaction rate. The polymerization rate of the Cu(II) complexes obtained from the kinetic experiment showed that steric and electronic effects of the ligand substituents slightly influenced catalytic activity though they are situated away from the metal center. Kinetic analysis of the carboxylate complexes showed a pseudo-first order relationship with respect to ε-CL and LAs as shown by the semi-logarithmic plot of ln([M]$_0$/[M]$_t$) *vs. t* in Fig. 4 and S30 – S32. This is in accordance with Eq. (3) where $k_{app} = k_p[I]^y$; k_p = rate of chain growth, I = initiator, and y = the order of reaction.

$$\frac{d[CL]}{dt} = k_{app}[M] \tag{3}$$

The kinetic analysis of the Zn(II) complexes showed that the polymerization rate of complex **5** (Table 3, entry 5) with a chloro substituent is higher than complexes **1** and **3** (Table 3, entries 1 and 3) with electron-donating substituents. Generally, the activity decreased with a decrease in electron withdrawing effects because of reduced metal nucleophilicity, which retarded monomer biding for activation. Related studies have also shown varying correlations between the substituents effects and activity using different ligands (García-Valle et al. 2015; Hornnirun et al. 2006; Nomura et al. 2002). The catalytic activity of the Cu(II) complexes followed the order: **7 > 2 > 9 > 12 > 4 > 13 > 10 > 8 > 11 > 6** showing that the polymerization rate of complexes **8** and **13** (Table 3, entries 8 and 13) with no substituent are higher than complexes **6** and **11** (Table 3, entries 6 and 11) with electron-withdrawing substituent but lower than complexes **2** and **9** (Table 3, entries 2 and 9) with electron-donating substituents. The polymerization rate of complexes **7** and **9** with less bulky *ortho* substituent are higher than complexes **4** and **10** with bulky *i*Pr substituent. Among the Cu(II) complexes, the polymerization rate of complex **7** with the *ortho*-substituted electron-donating methyl group had the highest. The steric hindrance in the ligand framework of a metal complex either decrease the catalytic activity by reducing the monomer coordination or increase it by stabilizing the active species (Qin et al. 2020; Wei et al. 2019). In this case, since the substituent are far from the metal center little crowding is expected. This can be observed from the slight difference in reaction rates of complexes **9** and **10**.
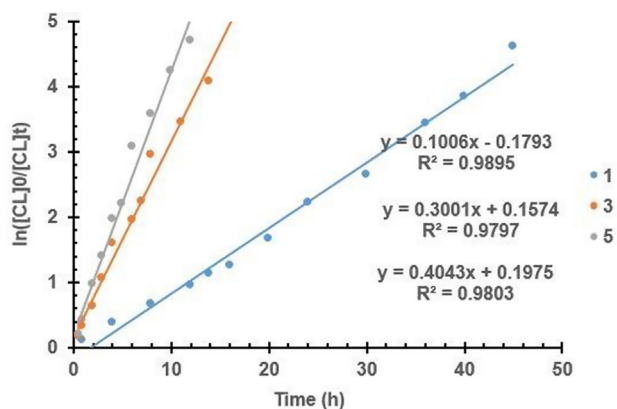

Fig. 4 Pseudo-first-order logarithmic plot for the bulk polymerization of CL at 110 °C by complexes **1**, **3** and **5**.

Complex **5** being the most active was selected for the polymerization of *rac*-LA and L-LA at 110 °C in toluene using a [monomer]/[catalyst] ratio of 200:1. A maximum conversion of 98 % was obtained between 5 and 9 h with an apparent rate constant (k_{app}) of 0.2513 h^{-1} and 0.1518 h^{-1} for *rac*-LA and L-LA polymerization, respectively (Fig. S30). The polymerization rate of *rac*-LA is higher than that of L-LA, a trend that has been reported (Pietrangelo et al. 2010). This has been linked to the ROP mechanism which favors racemic enchainment which is encoded by the monomer and/or the polymer stereocenters resulting in alternate D- and L-LA monomer insertion.

A plot of ln k_{app} *vs.* ln [**5**] using various catalyst concentrations at a fixed monomer concentration (Table 4) was employed to unravel the order of reaction with regards to complex **5**. The reaction order extracted from the slope of the line of best fit was found to be 0.75 (Fig. 5). Fast, polymerization kinetics have been reported mainly, using some zinc alkoxide (Stasiw et al. 2017) and in situ generated copper alkoxide catalyst (Kwon et al. 2015).

4.2. Effect of solvent and temperature on ε-CL polymerization

Complexes **5** and **7** (Zn(II) and Cu(II)) having superior activities were chosen as the model systems to understand better the structure (metal–ligand) effects on activity. Complex **5** was employed for the polymerization of ε-CL at different temperatures and complex **7** was used to investigate the effect of different alcohol co-initiators. The activity of complex **7** was further examined in the presence of different alcohol initiators at 110 °C using a [M]:[I]:[ROH] ratio of 200:1:1 (Fig. 6).

^{1}H NMR analysis of samples withdrawn at regular intervals confirmed the formation of alkoxide species (Fig. S33) which improved the catalytic activity obtained with benzyl alcohol, ethanol and isopropyl alcohol (Table 4 entries 7 – 9) relative to the bulk polymerization (Table 3 entry 9). The co-initiation trend followed the order EtOH > BnOH > t-BuOH, and this is consistent with reported trend using Sn(OR)$_2$ (Sattayanon et al. 2013; Sattayanon et al. 2015). From theoretical and available experimental data, they observed that the polymerization rate depends on three factors:hydrocarbon chain length, number and size of branched chains and number of coordinated alkoxide groups. An increase in hydrocarbon chain length, number and size of branched chains in the alkoxide results in greater steric hindrance thereby retarding monomer coordination. In addition, an increase in the number of coordinated -OR groups and the alkyl chain length decreases the positive charge of the nucleophilic center, hence making it less susceptible to monomer coordination resulting in reduced polymerization rates.

The molecular weight of PCL obtained with *t*-butanol co-initiator was higher than the other alcohol initiators even though it had the lowest activity recorded (Table 4 entry 10). This observation is linked to the steric hindrance present in the molecule. The molecular weight of PCL at 110 °C is much higher than that at lower temperatures 80 and 90 °C, at similar conversion. The lower Mw at lower temperature was a result of the long reaction times required which induced transesterification reactions, while at 110 °C the polymerization is quantitative after a shorter period (Stridsberg and Albertsson, 1999).

Table 4 Effect of temperature and co-initiator and solvent on the polymerization of ε-CL.[a]

Entry	Complex	[M]:[I]	ROH	Time (h)	Conv (%)	$^mM_{n\ (calc)}$ (kg mol^{-1})	$^nM_{n(NMR)}$ (kg mol^{-1})	k_{app} (h^{-1})
1	[b]**5**	200	–	80	84	19.6	1.33	0.0242
2	[c]**5**	200	–	42	98	22.4	1.60	0.0878
3	[d]**5**	200	–	26	97	22.4	1.82	0.1186
4	[e]**5**	200	–	12	99	22.6	3.08	0.4043
5	[h]**5**	200	–	23	99	22.6	2.30	0.2338
6	[i]**5**	200	BnOH	15	99	22.7	2.88	0.2903
7	[i]**7**	200	BnOH	24	99	22.7	0.96	0.2039
8	[j]**7**	200	EtOH	14	99	22.6	0.75	0.3202
9	[k]**7**	200	iPrOH	33	97	22.2	1.61	0.1466
10	[l]**7**	200	t-BuOH	50	96	22.0	2.83	0.0654

[a]Polymerization conditions: 110 °C in Bulk at [b]80 °C, [c]90 °C, [d]100 °C and [e]110 °C and in [h]toluene [i]Benzyl alcohol, [j]Ethanol, [k]Isopropyl alcohol and [l]tert-butano, [m]M_n calculated from the M_{wt} of monomer × [M]$_0$:[I]$_0$ × Conv. + [Mw $_{(chain-end\ group)}$], [n]Determined from NMR.
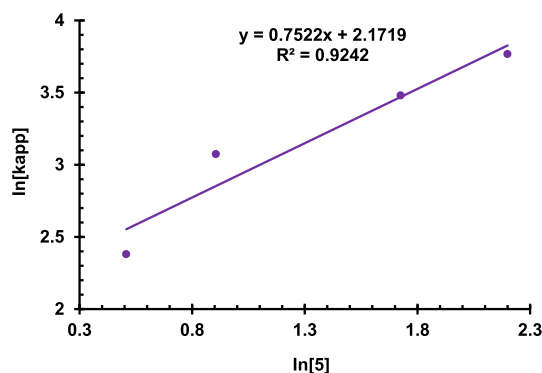


Fig. 5 Order of reaction determination from the plot of lnk_{app} against ln[**5**].
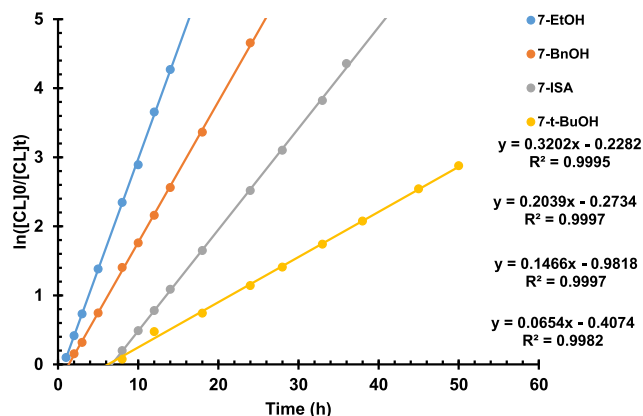
Fig. 6 Kinetic plots of ln[CL]$_0$/[CL]$_t$ vs. t for complex **7** in the polymerization of ε-CL using alcohol initiators.

The polymerization of ε-CL was examined at different temperatures (80 °C to 110 °C) using the most active zinc catalyst complex **5**. A marked reduction in the rate constant from 0.4043 h^{-1} at 110 °C to 0.0242 h^{-1} at 80 °C confirmed the temperature dependence of the reaction. Longer induction periods observed at 80 °C and 90 °C resulted in lower k_{app} of 0.0242 h^{-1} (Table 4 entry 1) and 0.0878 h^{-1} (Table 4 entry 2), respectively relative to the k_{app} of 0.1186 h^{-1} (Table 4 entry

3) and 0.4043 h^{-1} (Table 4 entry 4) obtained at 100 °C and 110 °C, respectively. An overall activation energy barrier (E$_a$) of 98.34 kJ mol^{-1} was obtained from the slope of the Arrhenius plot shown in Fig. 7. A large energy barrier of this magnitude is due to the strong M—O bond of the bridging acetate co-ligand (Munzeiwa et al., 2018). The enthalpy (ΔH) and entropy (ΔS) of activation were obtained from the slope of the Eyring plot as 95.28 kJ mol^{-1} and −7.47 JK^{-1} mol^{-1}, respectively, both of which conforms to an ordered transition (Fig. 7).

4.3. Molecular weight and molecular weight distribution of polymers.

The number molecular weight (M$_n$) and polydispersity index (ã) of PCL and PLA obtained from gel permeation chromatography (GPC) with adequate corrections as prescribed by Mark Houwink were compared to those obtained from ^{1}H NMR analysis and summarized in Table 5. Low M$_n$ polymers of 0.83–3.48 kg mol^{-1} and 1.28–2.39 kg mol^{-1} were obtained for PCL and PLA, respectively, with broad ã of 1.7–2.1 indicating a level of *trans*-esterification during the ROP reactions (Dubois et al. 1991). (Ikpo et al. 2012) The M$_n$ of the PCL obtained from GPC and NMR analysis increased as the [M]$_0$:[I]$_0$
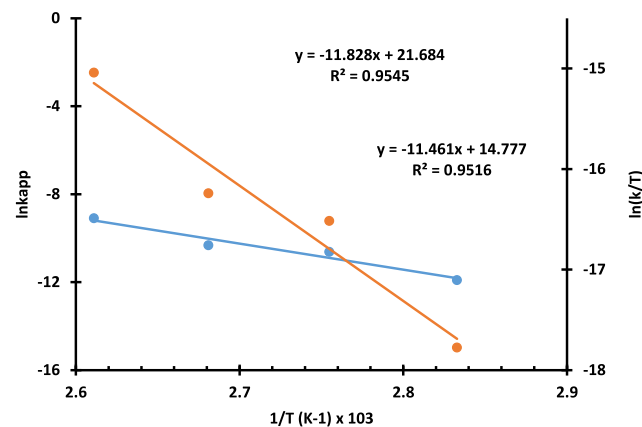
Fig. 7 Arrhenius plot of lnk vs T^{-1} and Eyring plot of ln(k_{app}/T) against T^{-1} for the bulk polymerization of ε-CL initiated by **5**.

Table 5 Molecular weight and molecular weight distribution of ε-CL and LAs by complex **5**[a].

| Entry	Complex	$[M]_0:[I]_0$	Time (h)	[c]Con (%)	[d]$M_{n(NMR)}$ (kg mol^{-1})	[e]$M_{n(GPC)}$ (kg mol^{-1})	[f]$\tilde{a}$
1	5	100	8	96	2.75	0.83	1.7
2	5	200	12	98	3.30	2.37	2.1
3	5	300	40	99	3.81	2.87	2.0
4	5	400	50	99	4.33	3.48	2.1
5	[a]5	200	20	95	1.27	1.28	1.7
6	[b]5	200	20	97	3.35	2.39	2.1

Polymerization of [a]$_L$-LA and [b]*rac*-LA in toluene at 110 °C, [c,d] Determined from NMR, [e,f]Obtained from GPC analysis and calibrated by polystyrene standard considering Mark-Houwink's corrections of 0.56 for CL and 0.58 for lactides.

increased from 100:1 to 400:1. This behavior can be alluded to the fact that there are few polymer chains propagating per initiating species at low catalyst loading, hence they grow much longer (Table 5 entries 1–4). The expected molecular weights slightly deviate from the experimental values obtained from GPC and NMR. This is as a result of self-termination intermolecular transesterification chain transfer reactions (*vide infra*) which kill the growing chains (Dubois et al. 1991; Ikpo et al. 2012). Also, molecular weights from GPC are comparable to those deduced from NMR and the inconsistency, hinges on separation mode in GPC which is based on polymer hydrodynamic volume rather than actual molecular weight (Balke and Cheng, 1991).

4.4. Stereochemistry of synthesized PLA

Homo-nuclear decoupled ^{1}H and ^{13}C NMR spectroscopy is an established technique for the structural analysis of PLA (Spassky et al. 1996). The tacticity of the PLA is obtained by inspection of the tetrad sequence of the methine region of the ^{1}H NMR in conjunction with the methine and carbonyl carbon region of the ^{13}C NMR (Fig. S36). Highly isotactic poly($_L$-LA) is produced by the ROP of $_L$-LA if no side reactions take place during polymerization. However, zinc based ROP of *rac*-LA resulted in isotactic PLAs which were dependent on the electronic effects of the para substituent (Stasiw et al. 2017). The Homo-nuclear decoupled ^{1}H NMR spectra of the synthesized PLA obtained from $_L$-LA by complex **5** (Fig. 8) revealed pure isotactic sequence (intense *iii* tetrad peak at 5.12 ppm) and a satellite peak at 5.16 ppm (sii/iis syndioatactic diads) pointing to metal induced racemization (Gadomska-Gajadhur and Ruśkowski, 2020). Similarly, the methine and carbonyl regions of the ^{13}C NMR were characterized by two signals observed at about 69.04 and 169.60 ppm, respectively (Fig. S36). Thus, we postulated that Zn(II) metal center in Shiff base complexes could induce racemization reactions by introducing the $_D$-LA monomer in the polymer chain thereby resulting in slight syndiotactic diads
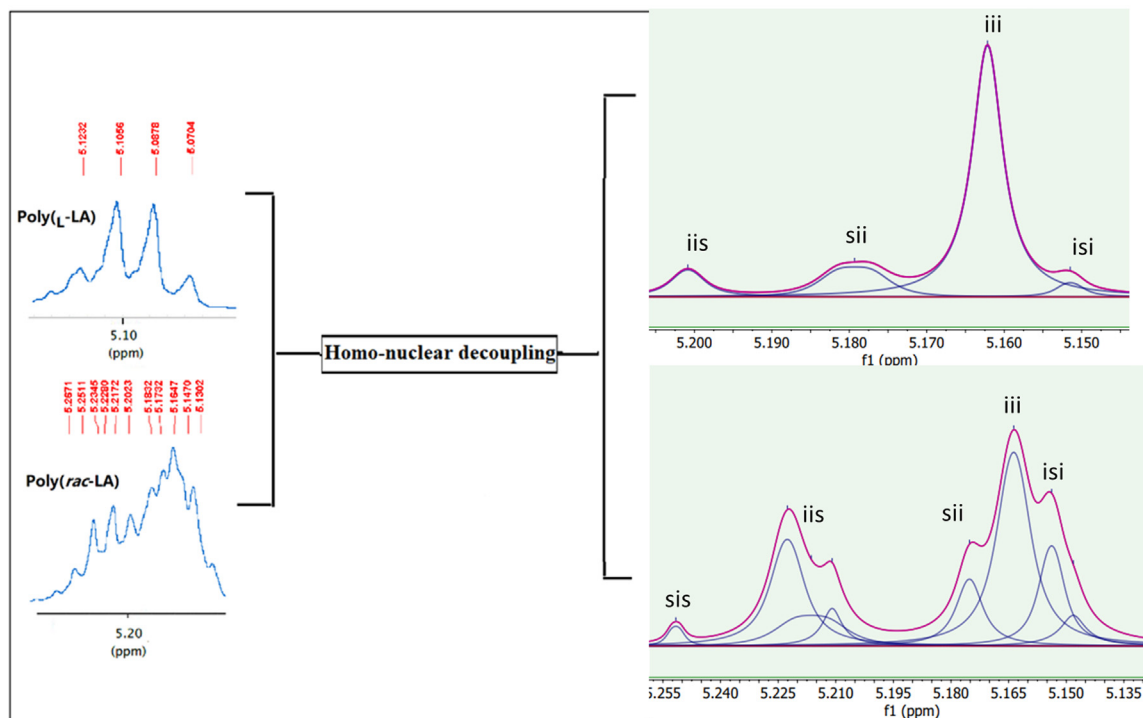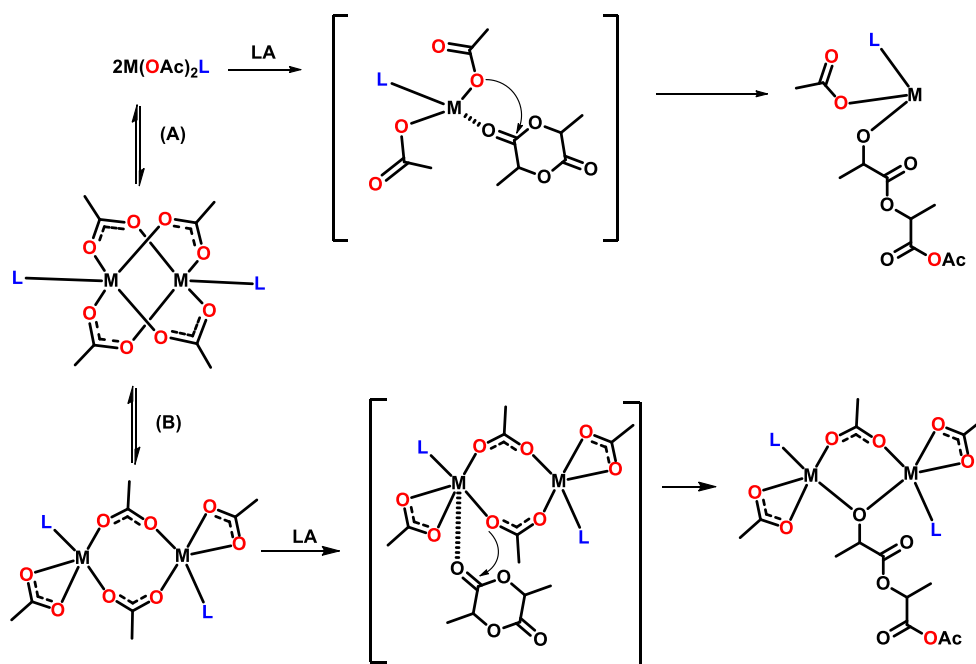

Fig. 8 Homo-nuclear decoupling of poly(LA) initiated by complex **5** at room temperature in CDCl$_3$ (400 MHz). Reaction conditions: $[CL]_0:[I]_0 = 200:1$, bulk, T = 110 °C.

(Gadomska-Gajadhur and Ruśkowski, 2020). With the *rac*-LA monomer the peaks observed in the range 5.15 – 5.17 ppm and 5.21 – 5.22 ppm in the decoupled ^{1}H NMR spectrum were assigned to *isi*, *iii*, *iis/sii* and *sii*, *iis* tetrads respectively (Fig. 8) (Chabot et al. 1983; Chisholm et al. 1999), which point to heterotactic PLAs with $P_r = 0.68$. The probability of heterotactic (P_r) enrichment was computed from intensities from homodecoupled ^{1}H NMR spectra, using the formula, $P_r = 2I_1/[I_1 + I_2]$, where $I_1 = (sis + sii)$ and $I_2 = (iis + iii + isi)$ (Cho et al., 2016; Honrado et al. 2015). The methine and carbonyl carbon peaks were observed at 69.02 and 169.19 ppm in the ^{13}C NMR spectrum (Fig. S36), confirming heteroatactic stereo-block PLA.

4.5. End group analysis and mechanistic study

The end group analysis and mechanism of ε-CL and LA polymerization obtained from ^{1}H NMR and ESI-MS analysis is majorly described by the activated monomer mechanism (AMM) and the coordination insertion mechanism (CIM) (Liu et al. 2009; Ajellal et al. 2010; Marlier et al. 2016). The AMM is characterized by the inclusion of an exogenous alcohol as a co-initiator, which activates the monomer upon coordination, whereas the CIM is characterized by the direct coordination of the cyclic ester monomer to the active site of the catalyst (Munzeiwa et al., 2019).

Scheme 3   Proposed mechanism pathways for ROP using paddlewheel acetate complexes.
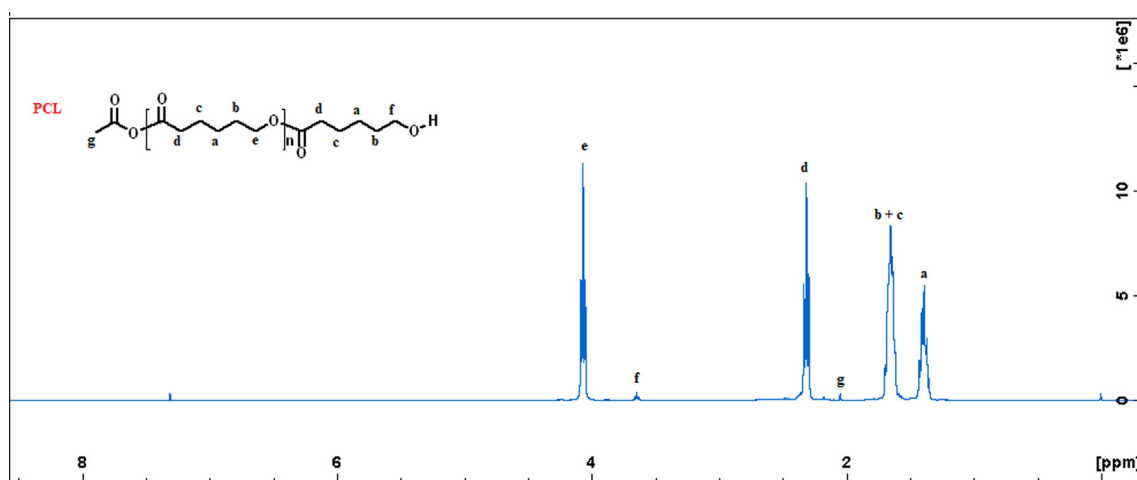
Fig. 9   The ^{1}H NMR spectrum of poly(ε-CL) initiated by complex **5** at room temperature in CDCl$_3$ (400 MHz). Reaction conditions: [CL]$_0$:[I]$_0$ = 200:1, bulk, T = 110 °C.

A CIM mechanism is proposed initially seeing the monomer becomes activated when the catalytic center generates a monomer-catalyst activated transition state that is preceded by insertion of monomer into the M—O bond; giving the first generation alkoxide macro initiator (Scheme 3). There are two possible initiation pathways for the paddlewheel complexes: the mononuclear (A) and binuclear (B). In the presence of an alcohol, path (A) is projected, where the two acetates would have been substituted by the alcohol to generate the alkoxide in *situ*. In a dinuclear indium system by Fang *et al* (Fang et al. 2013), a binuclear type preference was found to be the most probable pathway and they alluded the behavior to high energy barrier of dissociation to generate the active species. In order to understand, the preferred pathway, theoretical Density-functional theory (DFT) calculations are underway, and the details of which are not yet conclusive at this stage.

The ^{1}H NMR spectra of PCL and PLA synthesized using complex **5** (Figs. 9 and S34) revealed the OCH$_2$ peak at 3.65 and 4.87 ppm, respectively. The additional peak observed around 2.10 ppm was assigned to the methyl proton of the acetate capped to the end of the polymer. This observation points to a coordination insertion mechanism. Similarly, the ESI-MS analysis of the synthesized PLA obtained using complex **5** revealed fragment ions with successive peaks differing by a mass of 0.072.07 kg mol^{-1} corresponding to a half lactide unit (Fig. S35). For instance, a mass of 0.734 kg mol^{-1} contains a total of ten (n = 10) half lactide moiety in the polymeric chain (Fig. 9). Characteristic *m/z* peaks for other PCL and PLA in the presence and absence of alcohol initiators are provided in Figs. S39 – S42. However, the acetate group cannot be accounted in the ESI-MS, though it utilize soft ionization technique, collision-induced dissociation reaction may occur, and the anhydride can dissociate leading to the elimination of the acetate (Demarque et al. 2016).

5. Conclusion

A series of di-nuclear Zn(II) and Cu(II) complexes of pyridinyl Schiff base ligands were synthesized and characterized by IR, NMR, mass spectroscopy and elemental analysis. Single crystal X-ray diffraction studies of complexes **7**, **9**, **10** and **11** established that the complexes exhibit paddlewheel conformation with a distorted octahedral geometry around the Cu(II) centers. All complexes were active as catalysts in the bulk polymerization of ε-CL yielding low molecular weight polymers with broad *ã* due to intermolecular transesterification reactions. The presence of the electron-withdrawing chloro substituent seemed to increase activity for the Zn(II) complexes, whereas a decrease was observed for the Cu(II) complexes. On the other hand, the electron-donating methyl substituent favored higher activities with the Cu(II) complexes but lower for the Zn(II) analogue. The catalytic activities were slightly repressed by bulky isopropyl substituent at the *ortho* position, since they are far away from the catalytic center to effect reasonable steric impedance. The addition of alcohol co-initiators resulted in the formation of alkoxides species, which increased the catalytic activity obtained. However, a reduction of catalytic activity was obtained as the reaction temperature decreased from 110 °C to 80 °C. Complex **5** employed for the ROP of $_L$-LA afforded isotactic PLA while an heterotactic (Pr = 0.68) stereo-block was obtained with *rac*-LA.

References

Adeleke, A.A., Zamisa, S.J., Omondi, B., 2020. Crystal structure of dichlorido-bis ((E)-2-((pyridin-4-ylmethylene) amino) phenol) zinc (II), C24H20Cl2N4O2Zn. Zeitschrift für Kristallographie-New Crystal Structures 235, 625–628.

Ahn, S.H., Chun, M.K., Kim, E., Jeong, J.H., Nayab, S., Lee, H., 2017. Copper(II) complexes containing N, N′-bidentate N-substituted N-(pyridin-2-ylmethyl)amine: synthesis, structure and application towards polymerisation of rac-lactide. Polyhedron 127, 51–58.

Ajellal, N., Carpentier, J.-F., Guillaume, C., Guillaume, S.M., Helou, M., Poirier, V., Sarazin, Y., Trifonov, A., 2010. Metal-catalyzed immortal ring-opening polymerization of lactones, lactides and cyclic carbonates. Dalton Trans. 39, 8363–8376.

Akpan, E.D., Ojwach, S.O., Omondi, B., Nyamori, V.O., 2016a. Structural and kinetic studies of the ring-opening polymerization of cyclic esters using N, N′-diarylformamidines Zn(II) complexes. Polyhedron 110, 63–72.

Akpan, E.D., Ojwach, S.O., Omondi, B., Nyamori, V.O., 2016b. Zn (II) and Cu(II) formamidine complexes: structural, kinetics and polymer tacticity studies in the ring-opening polymerization of ε-caprolactone and lactides. New J. Chem. 40, 3499–3510.

Appavoo, D., Omondi, B., Guzei, I.A., van Wyk, J.L., Zinyemba, O., Darkwa, J., 2014. 'Bis(3,5-dimethylpyrazole) copper(II) and zinc (II) complexes as efficient initiators for the ring opening polymerization of ε-caprolactone and D L-lactides'. Polyhedron 69, 55–60.

Attandoh, N.W., Ojwach, S.O., Munro, O.Q., 2014. (Benzimidazolyl-methyl)amine Zn(II) and Cu(II) carboxylate complexes: structural, mechanistic and kinetic studies of polymerisation reactions of ε-caprolactone. Eur. J. Inorg. Chem. 2014, 3053–3064.

Balasanthiran, Vagulejan, Malcolm H. Chisholm, Kittisak Choojun, Christopher B. Durr, Pasco M. Wambua. 2016. 'BDI*MgX(L) where X = nBu and OtBu and L = THF, py and DMAP. The rates of kinetic exchange of L where BDI* = CH{C(tBu)N-2,6-iPr2C6H3}2', Polyhedron, 103, Part B: 235-40.

Balke, S.T., Cheng, H.N., 1991. In: Mays Barth, H.G., J. W (ed.), Modern Methods of Polymer Characterization (Wiley-Interscience: New York).

Bonné, C., Pahwa, A., Picard, C., Visseaux, M., 2017. Bismuth tris-silylamide: A new non-toxic metal catalyst for the ring opening (co-)polymerization of cyclic esters under smooth conditions. Inorganica Chim. Acta 455 (Part 2), 521–527.

Bruker (Ed.), 2009a. APEXII. APEXII Bruker AXS Inc, Madison, Wisconsin, USA.

Bruker (Ed.), 2009b. SADABS. Bruker SADABS Bruker AXS Inc, Madison,Wisconsin, USA.

Bruker (Ed.), 2009c. SAINT. SAINT Bruker AXS Inc, Madison, Wisconsin, USA.

Castro-Osma, Jose A., Alonso-Moreno, Carlos, Márquez-Segovia, Isabel, Otero, Antonio, Lara-Sánchez, Agustín, Fernández-Baeza, Juan, Rodríguez, Ana M., Sánchez-Barba, Luis F., García-Martínez, Joaquín C., 2013. Synthesis, structural characterization and catalytic evaluation of the ring-opening polymerization of discrete five-coordinate alkyl aluminium complexes. Dalton Transactions (Cambridge, England: 2003), 42, 9325–37.

Chabot, Francois, Vert, Michel, Chapelle, Stella, Granger, Pierre, 1983. Configurational structures of lactic acid stereocopolymers as determined by 13C{1H} NMR. Polymer 24, 53–59.

Chen, Hsuan-Ying, Mialon, Laurent, Abboud, Khalil A., Miller, Stephen A., 2012. Comparative study of lactide polymerization with lithium, sodium, magnesium, and calcium complexes of BHT. Organometallics 31, 5252–5261.

Chen, Lijuan, Li, Wenyi, Yuan, Dan, Zhang, Yong, Shen, Qi, Yao, Yingming, 2015a. Syntheses of mononuclear and dinuclear aluminum complexes stabilized by phenolato ligands and their applications in the polymerization of ε-caprolactone: A comparative study. Inorg. Chem. 54 (10), 4699–4708.

Chen, Yu-Hsieh, Chen, Yen-Jen, Tseng, Hsi-Ching, Lian, Cheng-Jie, Tsai, Hsin-Yi, Lai, Yi-Chun, Hsu, Sodio C.N., Chiang, Michael Y., Chen, Hsuan-Ying, 2015b. Comparing l-lactide and ?-caprolactone polymerization by using aluminum complexes bearing ketiminate ligands: steric, electronic, and chelating effects. RSC Adv. 5, 100272–100280.

Chisholm, Malcolm H., Iyer, Suri S., McCollum, David G., Pagel, Martin, Werner-Zwanziger, Ulrike, 1999. Microstructure of poly(lactide). phase-sensitive HETCOR spectra of poly(meso-lactide), poly(rac-lactide), and atactic poly(lactide). Macromolecules 32, 963–973.

Cho, Jaewon, Nayab, Saira, Jeong, Jong Hwa, 2016. Stereoselective polymerisation of rac-lactide catalysed by Cu(II) complexes bearing chloro derivatives of N, N′-bis(benzyl)dimethyl-(R, R)-1,2-diaminocyclohexane. Polyhedron 113, 81–87.

Colwell, John M., Wentrup-Byrne, Edeline, George, Graeme A., Schué, François, 2015. A pragmatic calcium-based initiator for the synthesis of polycaprolactone copolymers. Polym. Int. 64, 654–660.

D'Auria, Ilaria, Tedesco, Consiglia, Mazzeo, Mina, Pellecchia, Claudio, 2017. New homoleptic bis(pyrrolylpyridiylimino) Mg(II) and Zn(II) complexes as catalysts for the ring opening polymerization of cyclic esters via an "activated monomer" mechanism. Dalton Trans. 46, 12217–12225.

Demarque, Daniel P., Crotti, Antonio E.M., Vessecchi, Ricardo, Lopes, João L.C., Lopes, Norberto P., 2016. Fragmentation reactions using electrospray ionization mass spectrometry: an important tool for the structural elucidation and characterization of synthetic and natural products. Nat. Prod. Rep. 33 (3), 432–455.

Devaine-Pressing, Katalin, Lehr, Joshua H., Pratt, Michelle E., Dawe, Louise N., Sarjeant, Amy A., Kozak, Christopher M., 2015. Magnesium amino-bis(phenolato) complexes for the ring-opening polymerization of rac-lactide. Dalton Trans. 44, 12365–12375.

Dolomanov, Oleg V., Bourhis, Luc J., Gildea, Richard J., Howard, Judith A.K., Puschmann, Horst, 2009. OLEX2: a complete structure solution, refinement and analysis program. J. Appl. Crystallogr. 42, 339–341.

Dong, Yu-Wei, Fan, Rui-Qing, Chen, Wei, Zhang, Hui-Jie, Song, Yang, Xi, Du., Wang, Ping, Wei, Li-Guo, Yang, Yu-Lin, 2016. Luminescence properties of a Zn(ii) supramolecular framework:

easily tunable optical properties by variation of the alkyl substitution of (E)-N-(pyridine-2-ylethylidyne)arylamine ligands. RSC Adv. 6, 110422–110432.

Dubois, P., Jacobs, C., Jerome, R., Teyssie, P., 1991. Macromolecular engineering of polylactones and polylactides. 4. Mechanism and kinetics of lactide homopolymerization by aluminum isopropoxide. Macromolecules 24, 2266–2270.

El-Zoghbi, Ibrahim, Whitehorne, Todd J.J., Schaper, Frank, 2013. Exceptionally high lactide polymerization activity of zirconium complexes with bridged diketiminate ligands. Dalton Trans. (Cambridge, England: 2003), 42: 9376–9387.

Fang, Jian, Yu, Insun, Mehrkhodavandi, Parisa, Maron, Laurent, 2013. Theoretical investigation of lactide ring-opening polymerization induced by a dinuclear indium catalyst. Organometallics 32, 6950–6956.

Fliedel, Christophe, Rosa, Vitor, Alves, Filipa M., Martins, Ana M., Aviles, Teresa, Dagorne, Samuel, 2015. P, O-Phosphinophenolate zinc(ii) species: synthesis, structure and use in the ring-opening polymerization (ROP) of lactide, ?-caprolactone and trimethylene carbonate. Dalton Trans. 44, 12376–12387.

Fortun, Solène, Daneshmand, Pargol, Schaper, Frank, 2015. Isotactic rac-lactide polymerization with copper complexes: the influence of complex nuclearity. Angew. Chem. Int. Ed. 54, 13669–13672.

Gadomska-Gajadhur, Agnieszka, Ruśkowski, Paweł, 2020. Biocompatible catalysts for lactide polymerization—catalyst activity, racemization effect, and optimization of the polymerization based on design of experiments. Org. Process Res. Dev. 24, 1435–1442.

García-Valle, Francisco M., Estivill, Robert, Gallegos, Carlos, Cuenca, Tomás, Mosquera, Marta E.G., Tabernero, Vanessa, Cano, Jesús, 2015. 'Metal and ligand-substituent effects in the immortal polymerization of rac-lactide with Li Na, and K phenoxo-imine complexes. Organometallics 34 (2), 477–487.

Hong, Sungmin, Min, Kyung-Deok, Nam, Byeong-Uk, Park, O Ok, 2016. High molecular weight bio furan-based co-polyesters for food packaging applications: synthesis, characterization and solid-state polymerization. Green Chem. 18 (19), 5142–5150.

Honrado, Manuel, Otero, Antonio, Fernández-Baeza, Juan, Sánchez-Barba, Luis F., Garcés, Andrés, Lara-Sánchez, Agustín, Martínez-Ferrer, Jaime, Sobrino, Sonia, Rodríguez, Ana M., 2015. New Racemic and Single Enantiopure Hybrid Scorpionate/Cyclopentadienyl Magnesium and Zinc Initiators for the Stereoselective ROP of Lactides. Organometallics 34, 3196–3208.

Hormnirun, Pimpa, Marshall, Edward L., Gibson, Vernon C., Pugh, Robert I., White, Andrew J.P., 2006. Study of ligand substituent effects on the rate and stereoselectivity of lactide polymerization using aluminum salen-type initiators. Proc. Natl. Acad. Sci. 103, 15343–15348.

Ikpo, Nduka, Barbon, Stephanie M., Drover, Marcus W., Dawe, Louise N., Kerton, Francesca M., 2012. 'Aluminum methyl and chloro complexes bearing monoanionic aminephenolate ligands: synthesis, characterization, and use in polymerizations. Organometallics 31 (23), 8145–8158.

Jürgensen, Nils, Zimmermann, Johannes, Morfa, Anthony John, Hernandez-Sosa, Gerardo, 2016. Biodegradable polycaprolactone as ion solvating polymer for solution-processed light-emitting electrochemical cells. Sci. Rep. 6, 36643–36648.

Keram, Maryam, Ma, Haiyan, 2017. Ring-opening polymerization of lactide, ε-caprolactone and their copolymerization catalyzed by β-diketiminate zinc complexes. Appl. Organomet. Chem. 31, e3893–e3908.

Kireenko, Marina M., Kuchuk, Ekaterina A., Zaitsev, Kirill V., Tafeenko, Viktor A., Oprunenko, Yuri F., Churakov, Andrei V., Lermontova, Elmira Kh., Zaitseva, Galina S., Karlov, Sergey S., 2015. Aluminum complexes based on pyridine substituted alcohols: synthesis, structure, and catalytic application in ROP. Dalton Trans. 44 (26), 11963–11976.

Köppl, Alexander, Alt, Helmut G, 2000. Substituted 1-(2-pyridyl)-2-azaethene-(N, N)-nickel dibromide complexes as catalyst precur-

sors for homogeneous and heterogeneous ethylene polymerization. J. Mol. Catal. A: Chem. 154, 45–53.

Kumar, Umesh, Thomas, Jency, Thirupathi, Natesan, 2010. Factors dictating the nuclearity/aggregation and acetate coordination modes of lutidine-coordinated zinc (II) acetate complexes. Inorg. Chem. 49, 62–72.

Kwon, Kyuong Seop, Cho, Jaewon, Nayab, Saira, Jeong, Jong Hwa, 2015. Rapid and controlled polymerization of rac-lactide using copper(II) complexes of methyl-naphthalenylmethyl-(R, R)-1,2-diaminocyclohexanes. Inorg. Chem. Commun. 55, 36–38.

Li, Chen-Yu, Hsu, Shi-Jie, Lin, Chin-lung, Tsai, Chen-Yen, Wang, Jun-Han, Ko, Bao-Tsan, Lin, Chia-Her, Huang, Hsi-Ya, 2013. Air-stable copper derivatives as efficient catalysts for controlled lactide polymerization: Facile synthesis and characterization of well-defined benzotriazole phenoxide copper complexes. J. Polym. Sci., Part A: Polym. Chem. 51, 3840–3849.

Li, Wenbo, Xue, Mingqiang, Tu, Jing, Zhang, Yong, Shen, Qi, 2012. Syntheses and structures of lanthanide borohydrides supported by a bridged bis(amidinate) ligand and their high activity for controlled polymerization of ?-caprolactone, l-lactide and rac-lactide. Dalton Trans. 41, 7258–7265.

Liu, Jinzhi, Ling, Jun, Li, Xin, Shen, Zhiquan, 2009. Monomer insertion mechanism of ring-opening polymerization of ε-capro-lactone with yttrium alkoxide intermediate: A DFT study. J. Mol. Catal. A: Chem. 300, 59–64.

Liu, Junpeng, Ma, Haiyan, 2014. Aluminum complexes with bidentate amido ligands: synthesis, structure and performance on ligand-initiated ring-opening polymerization of rac-lactide. Dalton Trans. (Cambridge, England: 2003), 43, 9098–9110.

Liu, Xinli, Shang, Xiaomin, Tang, Tao, Ninghai, Hu., Pei, Fengkui, Cui, Dongmei, Chen, Xuesi, Jing, Xiabin, 2007. Achiral lanthanide alkyl complexes bearing N, O multidentate ligands. Synthesis and catalysis of highly heteroselective ring-opening polymerization of rac-lactide. Organometallics 26, 2747–2757.

Liu, Yi-Chang, Ko, Bao-Tsan, Lin, Chu-Chieh, 2001. A highly efficient catalyst for the "Living" and "Immortal" Polymerization of ε-Caprolactone and l-Lactide. Macromolecules 34, 6196–6201.

Marlier, Elodie E., Macaranas, Joahanna A., Marell, Daniel J., Dunbar, Christine R., Johnson, Michelle A., DePorre, Yvonne, Miranda, Maria O., Neisen, Benjamin D., Cramer, Christopher J., Hillmyer, Marc A., Tolman, William B., 2016. Mechanistic studies of ε-caprolactone polymerization by (salen)AlOR complexes and a predictive model for cyclic ester polymerizations. ACS Catal. 6, 1215–1224.

Mecking, Stefan, 2004. Nature or petrochemistry?—biologically degradable materials. Angew. Chem. Int. Ed. 43, 1078–1085.

Middleton, John C., Tipton, Arthur J., 2000. Synthetic biodegradable polymers as orthopedic devices. Biomaterials 21, 2335–2346.

Mittal, V., 2012. Renewable Polymers: Synthesis, Processing, and Technology. John Wiley & Sons, Hoboken, NJ.

Mosae Selvakumar, P., Nadella, S., Jashbanta Sahoo, Suresh, E., Subramanian, P.S., 2013. Copper(II) bis-chelate paddle wheel complex and its bipyridine/phenanthroline adducts. J. Coordination Chem., 66: 287–299.

Motreff, Artur, Correa, Rosenildo, da Costa, Hassan, Allouchi, Mathieu Duttine, Mathionière, Corine, Duboc, Carole, Vincent, Jean-Marc, 2012. A fluorous copper(II)–carboxylate complex which magnetically and reversibly responds to humidity in the solid state. J. Fluorine Chem. 134, 49–55.

Munzeiwa, Wisdom A., Nyamori, Vincent O., Omondi, Bernard, 2018. Zn(II) and Cu(II) unsymmetrical formamidine complexes as effective initiators for ring-opening polymerization of cyclic esters. Appl. Organomet. Chem. 32 (4), e4247. https://doi.org/10.1002/aoc.v32.410.1002/aoc.4247.

Munzeiwa, Wisdom A., Nyamori, Vincent O., Omondi, Bernard, 2019. N, O-Amino-phenolate Mg(II) and Zn(II) Schiff base complexes: Synthesis and application in ring-opening polymerization of ε-caprolactone and lactides. Inorg. Chim. Acta 487, 264–274.

Munzeiwa, Wisdom A., Omondi, Bernard, Nyamori, Vincent O., 2017. Synthesis and polymerization kinetics of ε-caprolactone and l-lactide to low molecular weight polyesters catalyzed by Zn(II) and Cu(II) N-hydroxy-N, N′-diarylformamidine complexes. Polyhedron 138, 295–305.

Nair, Lakshmi S., Laurencin, Cato T., 2007. Biodegradable polymers as biomaterials. Prog. Polym. Sci. 32, 762–798.

Nie, Kun, Fang, Lei, Yao, Yingming, Zhang, Yong, Shen, Qi, Wang, Yaorong, 2012. Synthesis and characterization of amine-bridged bis (phenolate) lanthanide alkoxides and their application in the controlled polymerization of rac-lactide and rac-β-butyrolactone. Inorg. Chem. 51 (20), 11133–11143.

Njogu, Eric M., Omondi, Bernard, Nyamori, Vincent O., 2017. Silver (I)-pyridinyl Schiff base complexes: Synthesis, characterisation and antimicrobial studies. J. Mol. Struct. 1135, 118–128.

Nomura, Nobuyoshi, Ishii, Ryohei, Akakura, Matsujiro, Aoi, Keigo, 2002. Stereoselective ring-opening polymerization of racemic lactide using aluminum-achiral ligand complexes: Exploration of a chain-end control mechanism. J. Am. Chem. Soc. 124, 5938–5939.

Nuñez-Dallos, Nelson, Posada, Andrés F., Hurtado, John, 2017. Coumarin salen-based zinc complex for solvent-free ring opening polymerization of ε-caprolactone. Tetrahedron Lett. 58, 977–980.

Pietrangelo, Agostino, Knight, Spencer C., Gupta, Aalo K., Yao, Letitia J., Hillmyer, Marc A., Tolman, William B., 2010. Mechanistic Study of the Stereoselective Polymerization of d, l-Lactide Using Indium(III) Halides. J. Am. Chem. Soc. 132, 11649–11657.

Qi, Yue, Luan, Yi, Yu, Jie, Peng, Xiong, Wang, Ge, 2015. Nanoscaled copper metal–organic framework (MOF) based on carboxylate ligands as an efficient heterogeneous catalyst for aerobic epoxidation of olefins and oxidation of benzylic and allylic alcohols. Chem.–A Eur. J. 21 (4), 1589–1597.

Qin, Lu, Cheng, Fangqin, Eisen, Moris S., Chen, Xia, 2020. Unexpected substituent's effects on catalytic activity in the ring-opening polymerization of ε-CL and δ-VL catalyzed by β-pyridyl-enamino Al complexes. Eur. Polym. J. 128, 109626. https://doi.org/10.1016/j.eurpolymj.2020.109626.

Range, Sven, Piesik, Dirk F.J., Harder, Sjoerd, 2008. Binuclear magnesium, calcium and zinc complexes based on bis(salicy-laldimine) ligands with rigid bridges. Eur. J. Inorg. Chem. 2008, 3442–3451.

Roberts, Courtney C., Barnett, Brandon R., Green, David B., Fritsch, Joseph M., 2012. Synthesis and structures of tridentate ketoiminate zinc complexes that act as L-lactide ring-opening polymerization catalysts. Organometallics 31, 4133–4141.

Rosal, Iker Del, Poteau, Romuald, Maron, Laurent, 2011. DFT study of the ring opening polymerization of ε-caprolactone by grafted lanthanide complexes: 2-Effect of the initiator ligand. Dalton Trans. 40 (42), 11228. https://doi.org/10.1039/c1dt10567a.

Sarma, R., Kalita, D., Baruah, J.B., 2009. Solvent induced reactivity of 3,5-dimethylpyrazole towards zinc (II) carboxylates. Dalton Trans. (Cambridge, England: 2003), 7428–7436.

Sattayanon, Chanchai, Kungwan, Nawee, Punyodom, Winita, Meep-owpan, Puttinan, Jungsuttiwong, Siriporn, 2013. Theoretical investigation on the mechanism and kinetics of the ring-opening polymerization of ε-caprolactone initiated by tin(II) alkoxides. J. Mol. Model. 19, 5377–5385.

Sattayanon, Chanchai, Sontising, Watit, Limwanich, Wanich, Meep-owpan, Puttinan, Punyodom, Winita, Kungwan, Nawee, 2015. Effects of alkoxide alteration on the ring-opening polymerization of ε-caprolactone initiated by n-Bu3SnOR: A DFT study. Struct. Chem. 26, 695–703.

Gerald, Scott, 2002. Why Degradable Polymers? In: Degradable Polymers. Springer.

Selvakumar, P. Mosae, Suresh, E., Subramanian, P.S., 2008. New macrocyclic Cu (II)-bischelates with paddle wheel Cu(II)-acetate cage. Inorganica Chim. Acta, 361, 1503–1509.

Sheldrick, G., 2008. Shelx. Acta Crystallogr Sect. A: Found. Crystal-logr. 64, 112–122.

Sheng, Hongting, Xu, Fan, Yao, Yingming, Zhang, Yong, Shen, Qi, 2007. Novel mixed-metal alkoxide clusters of lanthanide and sodium: synthesis and extremely active catalysts for the polymerization of ε-caprolactone and trimethylene carbonate. Inorg. Chem. 46, 7722–7724.

Sirajuddin, Muhammad, Ali, Saqib, McKee, Vickie, Matin, Abdul, 2020. Synthesis, characterization and biological screenings of 5-coordinated Organotin (IV) complexes based on carboxylate ligand. J. Mol. Struct. 1206, 127683.

Spassky, Nicolas, Wisniewski, Muriel, Pluta, Christian, Le Borgne, Alain, 1996. Highly stereoelective polymerization of rac-(D, L)-lactide with a chiral schiff's base/aluminium alkoxide initiator. Macromol. Chem. Phys. 197, 2627–2637.

Stasiw, Daniel E., Luke, Anna M., Rosen, Tomer, League, Aaron B., Mandal, Mukunda, Neisen, Benjamin D., Cramer, Christopher J., Kol, Moshe, Tolman, William B., 2017. Mechanism of the polymerization of rac-lactide by fast zinc alkoxide catalysts. Inorg. Chem. 56, 14366–14372.

Stridsberg, Kajsa, Albertsson, Ann-Christine, 1999. Ring-opening polymerization of 1,5-dioxepan-2-one initiated by a cyclic tin–alkoxide initiator in different solvents. J. Polym. Sci., Part A: Polym. Chem. 37, 3407–3417.

Sumrit, Pattarawut, Chuawong, Pitak, Nanok, Tanin, Duangthongyou, Tanwawan, Hormnirun, Pimpa, 2016. Aluminum complexes containing salicylbenzoxazole ligands and their application in the ring-opening polymerization of rac-lactide and ?-caprolactone. Dalton Trans. 45, 9250–9266.

Tanzi, Maria Cristina, Verderio, P., Lampugnani, M.G., Resnati, M., Dejana, E., Sturani, E., 1994. Cytotoxicity of some catalysts commonly used in the synthesis of copolymers for biomedical use. J. Mater. Sci. - Mater. Med. 5, 393–396.

Vagin, S., Ott, A.K., Rieger, B., 2007. Paddle-wheel zinc carboxylate clusters as building units for metal-organic frameworks. Chem. Ing. Tech. 79, 767–780.

Walton, Mark J., Lancaster, Simon J., Wright, Joseph A., Elsegood, Mark R.J., Redshaw, Carl, 2014. Zinc calixarene complexes for the ring opening polymerization of cyclic esters. Dalton Trans. 43, 18001–18009.

Wei, Chuanzhi, Han, Binghao, Zheng, Dejuan, Zheng, Quande, Liu, Shaofeng, Li, Zhibo, 2019. Aluminum complexes bearing bidentate amido–phosphine ligands for ring-opening polymerization of ε-caprolactone: steric effect on coordination chemistry and reactivity. Organometallics 38, 3816–3823.

Whitehorne, Todd J.J., Schaper, Frank, 2013. Square-planar Cu(II) diketiminate complexes in lactide polymerization. Inorg. Chem. 52, 13612–13622.

Wu, Jincai, Yu, Te-Liang, Chen, Chi-Tien, Lin, Chu-Chieh, 2006. Recent developments in main group metal complexes catalyzed/initiated polymerization of lactides and related cyclic esters. Coord. Chem. Rev. 250, 602–626.

Zhang, Chi, 2015. Biodegradable Polyesters: Synthesis, Properties, Applications. Biodegradable polyesters, Wiley-VCH, Weinheim.

Zhang, Yunping, Gao, Aihong, Zhang, Yongfang, Xu, Zhenghe, Yao, Wei, 2016. Aluminum complexes with benzoxazolphenolate ligands: Synthesis, characterization and catalytic properties for ring-opening polymerization of cyclic esters. Polyhedron 112, 27–33.

Zhu, Qin-Yu, Liu, Yu, Lu, Zhe-Jun, Wang, Jin-Po, Huo, Li-Bin, Qin, Yu-Rong, Dai, Jie, 2010. A paddlewheel dinuclear Cu(II) compound coordinated with TTF-py redox ligand. Synth. Met. 160, 713–717.

Zikode, Mnqobi, Ojwach, Stephen O., Akerman, Matthew P., 2016. Bis(pyrazolylmethyl)pyridine Zn(II) and Cu(II) complexes: Molecular structures and kinetic studies of ring-opening polymerization of ε-caprolactone. J. Mol. Catal. A: Chem. 413, 24–31.